Journal of Medicinal Chemistry

Article

pubs.acs.org/jmc

Novel Spiroketal Pyrrolidine GSK2336805 Potently Inhibits Key Hepatitis C Virus Genotype 1b Mutants: From Lead to Clinical Compound

Wieslaw M. Kazmierski,* Andrew Maynard, Maosheng Duan,† Sam Baskaran, Janos Botyanszki, Renae Crosby, Scott Dickerson, Matthew Tallant, Rick Grimes, Robert Hamatake, Martin Leivers, Christopher D. Roberts, and Jill Walker

GlaxoSmithKline, 5 Moore Drive, Research Triangle Park, North Carolina 27709-3398, United States

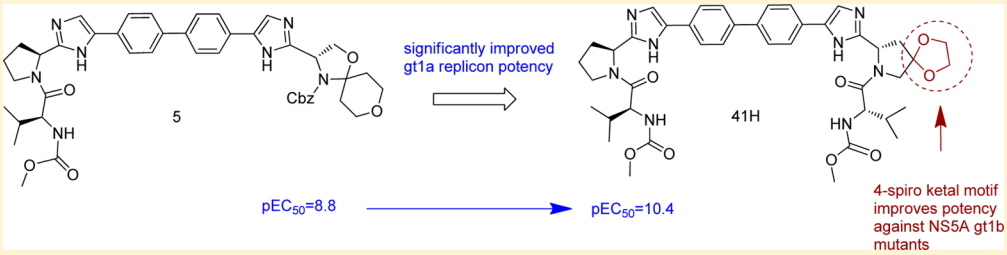

ABSTRACT: Rapid clinical progress of hepatitis C virus (HCV) replication inhibitors, including these selecting for resistance in the NS5A region (NS5A inhibitors), promises to revolutionize HCV treatment. Herein, we describe our explorations of diverse spiropyrrolidine motifs in novel NS5A inhibitors and a proposed interaction model. We discovered that the 1,4-dioxa-7-azaspiro[4.4]nonane motif in inhibitor **41H** (GSK2236805) supported high potency against genotypes 1a and 1b as well as in genotype 1b L31V and Y93H mutants. Consistent with this, **41H** potently suppressed HCV RNA in the 20-day RNA reduction assay. Pharmacokinetic and safety data supported further progression of **41H** to the clinic.

INTRODUCTION

Hepatitis C virus (HCV) affects more than 170 million individuals worldwide.[1] About 80% of all HCV infections become chronic and can lead to fibrosis, cirrhosis, and hepatocellular carcinoma.[2,3] Until recently, a combination of injectable peginterferon and oral ribavirin had been the standard of care for the treatment of HCV infection. The use of interferon can cause unpleasant flulike symptoms and fatigue, resulting in significant treatment discontinuations and failure. The recently introduced HCV protease inhibitors increased the sustained viral response (SVR), considered a virologic cure, for both treatment-naive and experienced patients. In addition, rapid clinical development of other anti-HCV agents, including NS5A inhibitors, promise a tantalizing opportunity for an all-oral, non-interferon HCV therapy in the near future.[4−6]

Daclatasvir (BMS-790052, **6**) is the first-reported NS5A inhibitor with high potency in both HCV genotype 1a (gt1a) and HCV genotype 1b (gt1b) (Table 1).[7,8] In their elegant and insightful work, BMS scientists identified potent "dimeric" HCV inhibitors in the mixture of biologically active species obtained by incubating the monomeric iminothiazolidinone HCV inhibitor BMS-824 in a cell culture medium.[9] Removal of the iminothiazolidinone moiety from dimeric products resulted in potent *trans*-stilbene class of inhibitors,[10] which through several other series[11,12] led to "dimeric" biphenyl scaffold in **6**.[7,8] Additional NS5A inhibitors from a number of laboratories have been reported in patent and scientific literature.[13−15]

Table 1. Potencies of 1−6b in gt1a and gt1b Replicon Assays[a]

	replicon pEC_{50}	
compd	gt1a	gt1b
1	<4.7	5.6
2	<4.7	6.9
3	<4.7	9.6
4	8.8	11.2
5	8.8	11.7
6	10.4	11.0
6a	6.3	6.7
6b	6.1	6.9

[a] $pEC_{50} = -\log EC_{50}$.

Our own medicinal chemistry efforts followed the initial hit **1** discovered through high throughput HCV replicon screen (Figure 1).[16] The combination of attractive pEC_{50} in gt1b HCV replicon assay[17] and low molecular weight supported further optimization efforts. Further derivatization of **1** with the *p*-cyclopropylcarboxamide moiety resulted in compound **2** and about 10-fold potency improvement in replicon gt1b assay. Subsequent use of the aromatic amide and spiroproline motifs in compound **3** brought about additional and substantial potency

Special Issue: HCV Therapies

Received: August 26, 2013
Published: February 26, 2014

dx.doi.org/10.1021/jm4013104 | *J. Med. Chem.* 2014, 57, 2058−2073

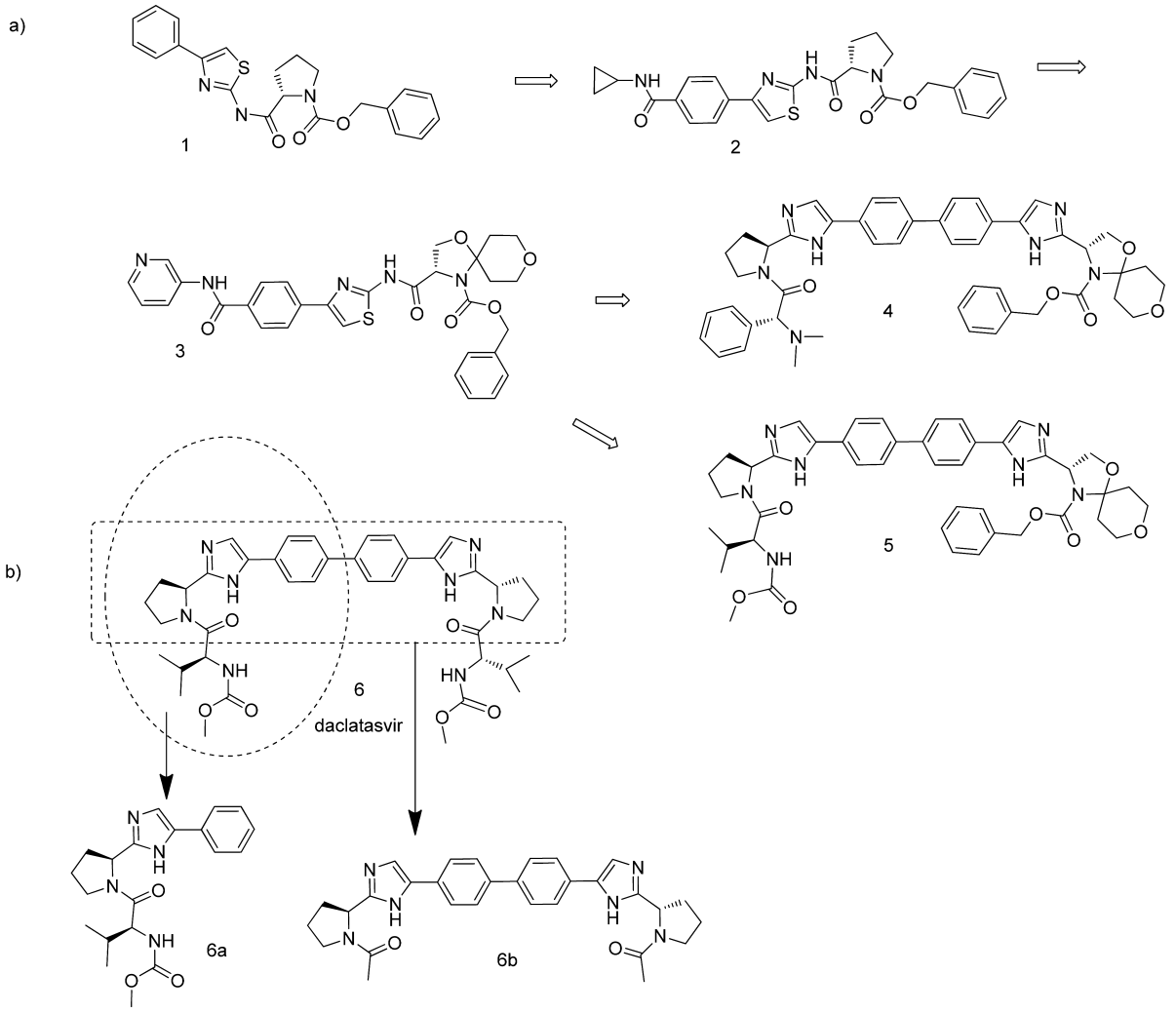

Figure 1. (a) Evolution of monomeric ligand **1** into pseudo-dimeric **4** and **5**. (b) Less potent fragments: "monomer" **6a** and truncated peptidic caps **6b**.

increase in replicon gt1b but not gt1a. Enhancing the latter proved challenging but could be accomplished by incorporating the biphenyl motif in spirooxazolidines **4** and **5** (Figure 1).[18,19]

PUTATIVE BINDING MODE OF DIMERIC NS5A INHIBITORS

The exact mechanism(s) of HCV inhibition by NS5A inhibitors remains a subject of ongoing investigations.[14,20−23] Assigning NS5A as the target of synthetic inhibitors has been complicated by the lack of definitive NS5A functional assays, as well as the lack of observed inhibitor−NS5A binding using purified NS5A, in isolation from the HCV replication complex (RC). However, mutation data and chimera studies map the sensitivity of HCV inhibition to the N-terminus of NS5A, particularly residue positions 30, 31, and 93, in the case of dimeric inhibitors.[7,21,22] Moreover, application of biotin-tagged and photoaffinity labeled inhibitors in protein pull-down experiments implicates association between dimeric inhibitors and NS5A in the functional context of the cellular RC.[22,23] Cell-based phenotypic studies also demonstrated that dimeric HCV inhibitors induce relocalization of NS5A from the endoplasmic reticulum to lipid droplets in replicon 1b cells, concomitant with the onset of replicon inhibition.[22] Inhibitor action was interpreted as the binding of a NS5A site during de novo RC formation which conformationally restricts NS5A, preventing sequestration to and promotion of RC formation, resulting in inert localization of NS5A to lipid droplet (LD) surfaces.

Consistent with the lack of observed interactions between inhibitors and purified NS5A in isolation, no NS5A inhibitor cocrystal structures have been published to date. Two published structures of the N-terminal NS5A zinc finger (ZnF) domain reveal formation of a homodimer, although the relative arrangements of the monomer units are quite different, suggesting the possibility of multiple protein−protein or protein−RNA interaction roles of NS5A.[24,25] Symmetry suggests dimeric inhibitors interact with a dimeric form of NS5A, experimentally supported by dimeric NS5A pull-down, cross-linked with a dimeric bis-azide inhibitor (BMS-351).[23] Utilizing the Love et al. structure, which was more consistent with internal data, manual docking of dimeric inhibitors (S. Dickerson, unpublished) suggested a C_2-symmetric orientation of inhibitors along the dimer interface (Figure 2) that is distinct from recently published docking studies[23] utilizing the Tellinghuisen et al. structure. To better understand the context of loop mutations (sites 28, 30, 31), the relative orientation of the N-terminal α-helices and differential monomeric vs dimeric inhibitor SAR, a NS5A gt1b domain I homology model was subsequently constructed by splicing the ZnF domain (aa 33−191)[25] and N-terminal amphiphilic α-helix (aa 1−31)[26] units.[14] Our model suggests a symmetric binding mode of **5** along the dimer

dx.doi.org/10.1021/jm4013104 | J. Med. Chem. 2014, 57, 2058−2073

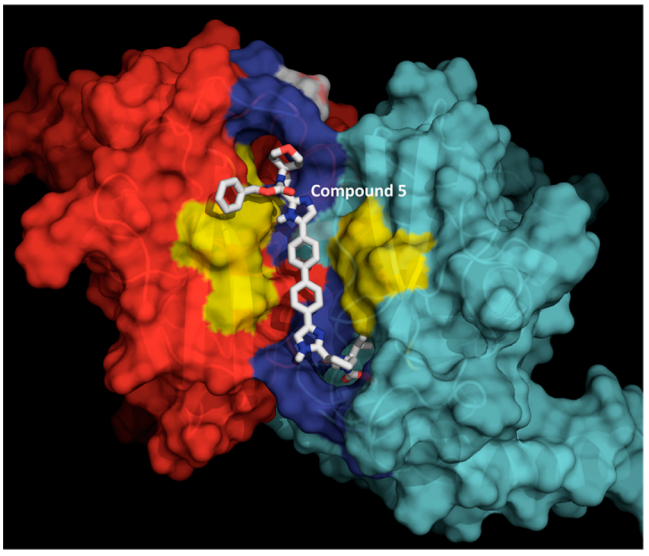

Figure 2. Putative binding mode of compound **5** with NS5A gt1b domain I. Compound **5** (sticks, white carbons) spans the dimer interface, positioning the peptidic caps in the cavities formed between the ZnF domain and N-terminal α-helix units of the NS5A homodimer. The monomer units of the homodimer are color-coded red and cyan. Reported daclatasvir resistant mutation sites (gt1a, M28T, Q30H/R, L31M, Y93C; gt1b, L31V, Y93H),[7] color-coded blue, border the terminal peptidic caps of dimeric inhibitors. In contrast, gt1a/gt1b residue differences (H/Q54, R/T56, H/P58, E/Q62), color-coded yellow, are located along the central dimer interface, flanking the inhibitor biaryl core.

interface whereby the amino acid moieties of **5** interact with cavities formed by the connecting protein loops (aa 27−37) at the ZnF and N-terminal α-helix junctions (Figure 2). The biaryl spacing of the inhibitor core is also consistent with the distance between the resistant mutations[7] at the dimer interface (blue, Figure 2). The model suggests that the peptidic "caps" of dimeric compounds, including **5**, make buried contacts at the dimer interface, where resistant mutations are prevalent. The proposed binding mode would restrict the movement of the N-terminal α-helix relative to the ZnF domain, presumably impairing the cis-acting function reported for NS5A.[27] This binding mode could lock NS5A in an inactive conformational state, as attributed to relocalization of NS5A from RC to LD.[22] Furthermore, the model provides a rationale for dimeric inhibitors; considering the peptidic caps as individually bound fragments, cooperative delivery of the caps (via a biaryl core spanning the interface) yields an exponential increase in affinity: $K_{d,dimer} = \exp[-\Delta G_{dimer}/(RT)] \approx \exp[-2\Delta G_{monomer}/(RT)] = K_{d,monomer} \times K_{d,monomer}$. The (buried) peptidic caps primarily drive the potency, while the core endows cooperative binding. Thus, weakly bound caps ($K_{d,monomer} \approx 10\ \mu M$), when spatially coupled, result in high-affinity inhibitors ($K_{d,dimer} \approx K_{d,monomer} \times K_{d,monomer} \approx 0.1$ nM). Accordingly, a sharp drop in potency is observed with "monomeric" (**6a**) or "truncated peptidic cap" (**6b**) compounds (Figure 1, Table 1). This is also consistent with picomolar potencies of dimeric HCV NS5A inhibitors containing a variety of central cores of similar lengths, including biphenyl, benzimidazole, napthyl, quinoline, isoquinoline, and other rigid cores synthesized in our NS5A program.[28−30] While the model

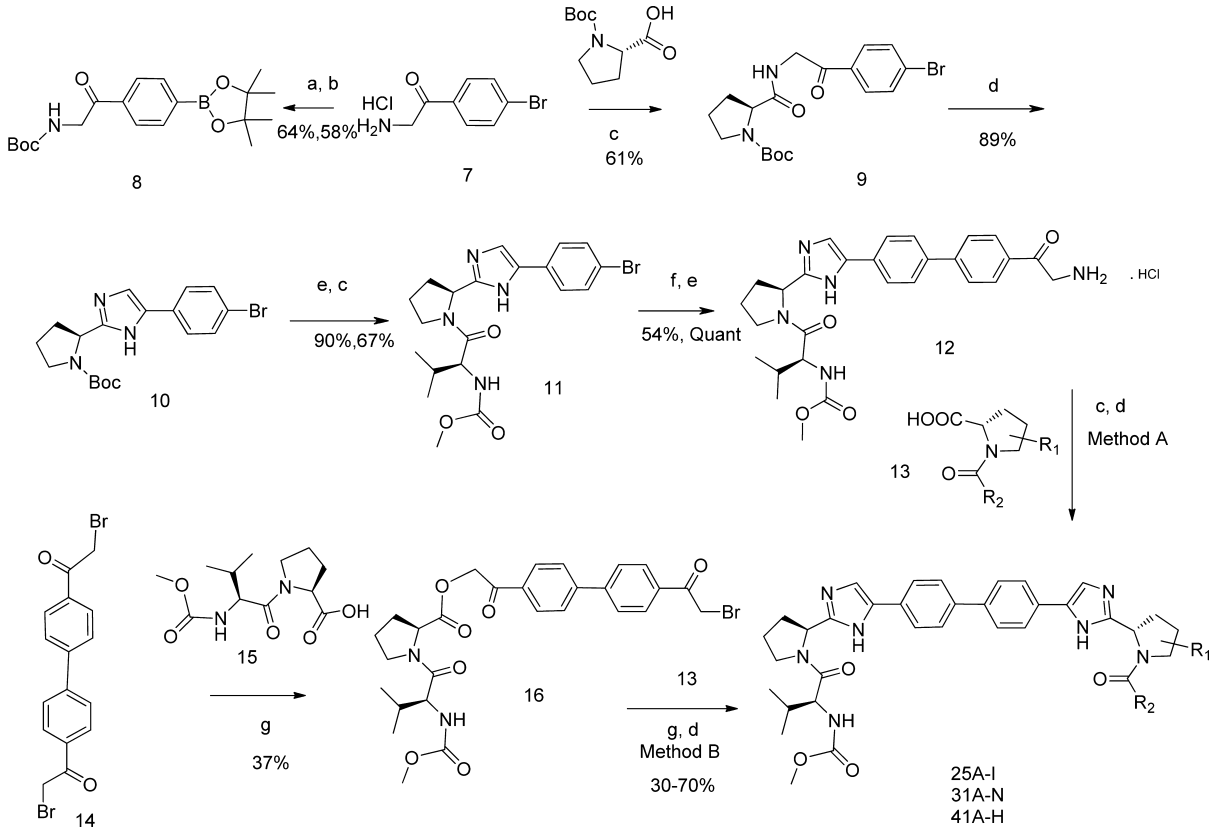

Figure 3. Synthesis of inhibitors. Reagents and conditions are as follows: (a) dioxane, Et_3N, Boc_2O; (b) dioxane, $Pd(dppf)Cl_2$, bis(pinacolato)diboron, KOAc; (c) CH_2Cl_2, HATU, DIEA, acid component; (d) NH_4OAc, dioxane, 110 °C, 48 h or microwave 160 °C, 20 min; (e) HCl_{aq}; (f) DME, $NaHCO_3$, $Pd(dppf)Cl_2$, 18h, 80 °C, **8**; (g) DMF, NaH, rt, 15 min Et_3N, acid component.

dx.doi.org/10.1021/jm4013104 | J. Med. Chem. 2014, 57, 2058−2073

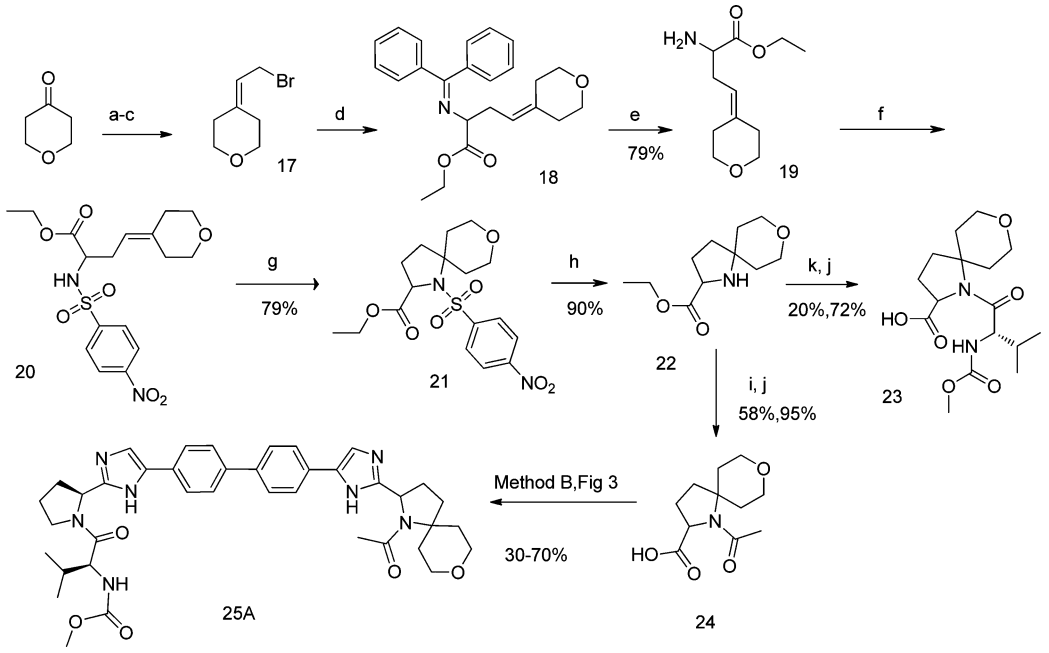

Figure 4. Synthesis of 5-spiropyrrolidines. Reagents and conditions are as follows: (a) THF, triethylphosphonoacetate, NaH; (b) CH_2Cl_2, DIBAL-H; (c) THF, CBr_4, triphenylphosphine; (d) CH_2Cl_2, $BnEt_3NCl$, CsOH, ethyl 2-(diphenylmethyleneamino)acetate; (e) CH_3COOH, THF, water; (f) CH_2Cl_2, Hunig's base, 4-nitrobenzene-1-sulfonyl chloride; (g) TfOH, $CHCl_3$; (h) K_2CO_3, CH_3CN, 18-crown-6, benzenethiol; (i) CH_2Cl_2, DIEA, acetyl chloride; (j) LiOH, THF/MeOH/water; (k) AgCN, rt, CH_2Cl_2, overnight, carboxymethylvaline chloride (CM-Val-Cl).

supports cooperative binding of the peptidic caps via a biaryl-like spacer, it also suggests that the binding of both caps is not necessarily equivalent, depending on the spacing of the caps.

Although there is strong homology (84% identity) between gt1a and gt1b in NS5A domain I, gt1a/gt1b residue differences M/L28, Q/R30, I/V34, V/F37, H/Q54, R/T56, H/P58, and E/Q62 (yellow, Figure 2) are of a particular interest because of their proximity to the putative binding pocket. H/Q54 and R/T56 are located in the β-sheet flanking the central binding channel, while H/P58 is strategically located in a short β-sheet loop at the entrance of the binding cavities. Biaryl cores in dimeric inhibitors possibly take advantage of aromatic−aromatic and/or cation−aromatic interactions with gt1a residues H54 and R56, leading to potency enhancement in the gt1a replicon assay. Additional gt1a/gt1b residue variants M/L28 and Q/R30 are located in the flexible protein loop region. We propose that gt1a/gt1b residue differences in the binding channel (H/Q54, R/T56, and H/P58), in concert with M/L28 and Q/R30 in the flexible loop region, may cause the observed differential gt1a and gt1b potency profiles of NS5A inhibitors, as observed in Table 1. As potential experimental validation of this model, it would be interesting to swap these residues between respective NS5A gt1a and gt1b constructs to test if this inverts the observed gt1a and gt1b potency profiles of NS5A inhibitors. Such experiments would provide circumstantial validation of proposed binding models in the absence of cocrystal data.

A number of mutations in both wt gt1a (M28T, Q30H/R, L31M, Y93C) and gt1b (L31V, Y93H) have been reported to lead to significant viral resistance.[31] In the model, these residue positions (blue, Figure 2) surround the terminal peptidic caps. Notably, the proline position of the inhibitor scaffold was considered of key importance, since it is surrounded by all four positions (28, 30, 31, and 93). The proline position also restricts the conformational flexibility of the inhibitor scaffold, orienting the peptidic caps to make buried contacts within the dimer interface at right angles to the central core. Since both gt1b resistant mutations L31V and Y93H result in smaller residues, possibly causing reduced interactions with the peptidic caps in **6** (Table 6), we also speculated that bulkier pyrrolidines in dimeric inhibitors could potentially restore interactions with these mutants and improve potency in gt1b L31V and Y93H replicon assays.

In this work we present the synthesis and evaluation of diverse spiropyrrolidine motifs designed to address the potency issues against gt1b L31V and L93H mutants, leading to the discovery of the clinical HCV inhibitor **41H** (GSK2336805).[28]

RESULTS AND DISCUSSION

5-Spiro Inhibitors. On the basis of our initial modeling considerations and SAR, we designed additional 5-spiropyrrolidine analogues (Table 2). These inhibitors were synthesized by coupling appropriate acid components to key intermediates, amine **12** or bromide **16**, followed by imidazole cyclization (Figure 3).

The 5-spiropyrrolidines in Table 2 were synthesized in a manner analogous to the synthesis of tetrahydropyran **22** (Figure 4). Thus, the alkylation of glycine synthon with bromide **17** was used to secure ester **18**. Next, the protecting groups were swapped in **18** via intermediate amine **19**, resulting in the sulfonamide **20**, which was then cyclized to the desired 5-spirotetrahydropyran **21**. Finally, thiol-mediated cleavage of the sulfonamide protecting group afforded racemic **22** (Figure 4).[32,33]

Acylation of amine **22** with acetyl chloride proceeded as expected, yielding **24** after ester hydrolysis. Acid **24** was then coupled to **16** and the product cyclized to imidazole **25A**. However, attempts to acylate **22** with more sterically hindered acids, such as Boc-valine or carboxymethylvaline (CM-Val), failed to yield the desired product under many standard amide coupling conditions (not shown). We established that products,

dx.doi.org/10.1021/jm4013104 | J. Med. Chem. 2014, 57, 2058−2073

such as **23**, can be synthesized via the acyl chlorides (e.g., CM-Val-Cl) route in the presence of silver cyanide (Figure 4), and we used this procedure in further syntheses.

In the R_2 = acetyl series, the use of spirotetrahydropyran moiety in **25A** resulted in a superior gt1b and gt1a profile compared to the difluorocyclohexane moiety in **25B** (Table 2). Larger R_2 = Cbz in **25C** proved to be deleterious to gt1a potency vs **25A**. In the context of R_2 = carboxymethylvaline, the sulfone moiety in **25D** clearly was a less attractive spiro partner, compared to both spirotetrahydropyran (**25E**) and difluorocyclohexane (**25F**), which on the other hand were equivalent. In addition, incremental amino acid side chain variations in the R_2 (in the context of spirodifluorocyclohexanes **25F–I**) had only minor effect on potency, but similar to **25A**, lower molecular volume of alanine in **25H** appeared to be somewhat advantageous to the overall potency. Thus, especially in the context of gt1a, this series favors the tetrahydropyran and difluorocyclohexane spiro moieties and small R_2. Compounds **25A** and **25H** were more potent in gt1a replicon than lead molecules **4** and **5**, encouraging us to explore additional spirocyclic motifs.

Table 2. Gt1a and gt1b Replicon Potencies of 25A–I

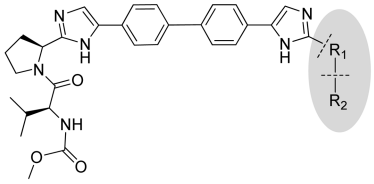

Compound	R_1	R_2	replicon pEC_{50} Gt 1a	Gt 1b
25A	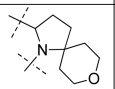		9.5	10.9
25B	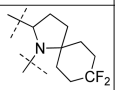		7.6	10.0
25C	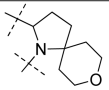	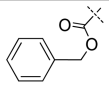	8.2	11.2
25D	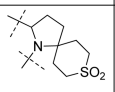	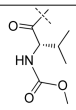	7.9	9.5
25E	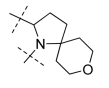	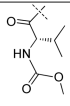	8.8	10.2
25F	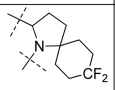	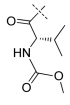	8.8	10.8
25G	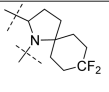	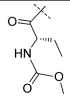	9.0	10.8
25H	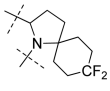	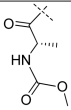	9.2	11.0
25I	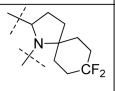	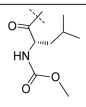	8.7	10.9

4-Spiro Non-Ketal Inhibitors. We next focused on the 4-spiropyrrolidine motif, exemplified here with inhibitors **31A–N** (Table 3). The general approach to compounds in this series is illustrated with the synthesis of **31G** (Figure 5). Thus, the reaction of enamine **27** and oxime **28** was used to generate the oxazine **29**. Subjecting the latter to the RaNi-mediated ring contraction provided the racemic ester **30**.[34] Subsequent chemistry toward **31G** utilized steps described in Figure 3. Inhibitors **31A** and **31C–N** were synthesized in a similar manner as diastereomeric mixtures. We later established chromatographic conditions toward separating enantiomers in **30** and via the dipeptide **32** were able to synthesize **43A** as a single isomer (Table 5).

Table 3. gt1a and gt1b Replicon Potencies of 31A–N[a]

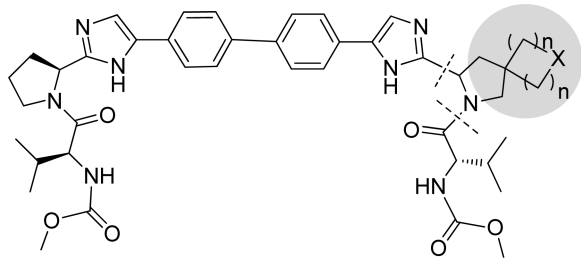

compd	X	*n*	replicon pEC_{50} gt1a	gt1b
31A	SO_2	2	9.4	10.4
31B[b]	CF_2	2	10.4	11.6
31C	N-Boc	2	8.0	10.4
31D	NH	2	<7.5	8.8
31E	N-Ac	2	8.0	9.7
31F	N-COOMe	2	9.1	10.8
31G	O	2	10.2	10.8
31H	N-Boc	1	9.0	11.0
31I	NH	1	8.5	9.9
31J	N-Ac	1	8.9	9.8
31K	N-COOMe	1	8.7	10.3
31L	N-CONHMe	1	8.2	9.6
31M	N-SO_2Me	1	8.9	10.3
31N	CF_2	1	10.0	11.4

[a]All compounds in this table are diasteromeric mixtures except **31B**. [b]**31B** is a single (*S*)-spiropyrrolidine isomer.

Toward the synthesis of inhibitor **31B**, the initial conversion of silyl ether **33** to ketone **34** and treatment with the Deoxo-Fluor resulted in a difficult to separate mixture of **35** (and its *R*-enantiomer) and the byproduct **36**. To facilitate the purification, crude mixture was treated with mCPBA, a step that converted **36** to a more readily separable epoxide (not shown), followed by facile chiral chromatography purification. Conversion of

dx.doi.org/10.1021/jm4013104 | J. Med. Chem. 2014, 57, 2058–2073

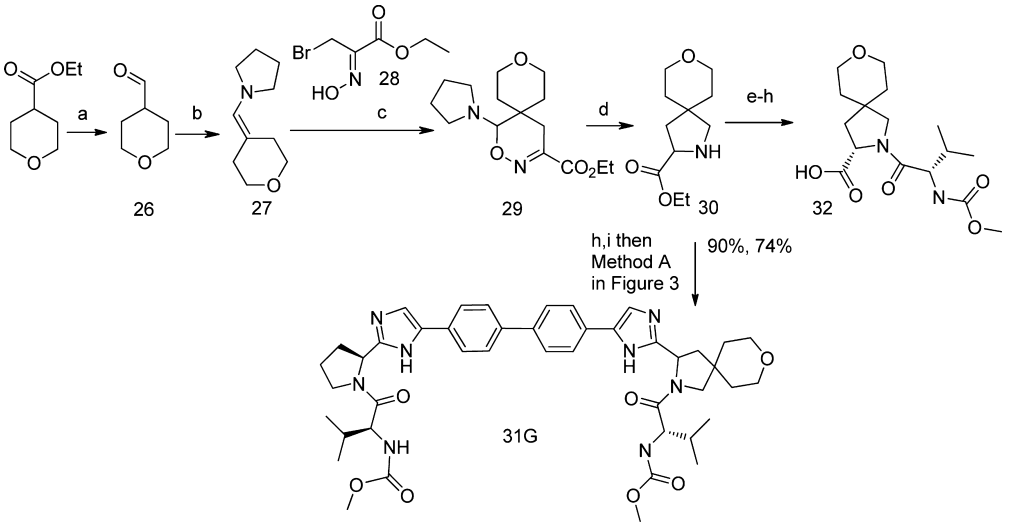

Figure 5. Synthesis of **31G**. Reagents and conditions are as follows: (a) CH_2Cl_2, DIBAL-H; (b) benzene, pyrrolidine, reflux; (c) THF, Et_3N; (d) EtOH, Raney nickel, H_2; (e) CH_2Cl_2, CBz-Cl, Et_3N; (f) chiral separation; (g) $Pd(OH)_2$, H_2, (h) CH_2Cl_2, HATU, DIEA, acid; (i) LiOH, THF/MeOH/water.

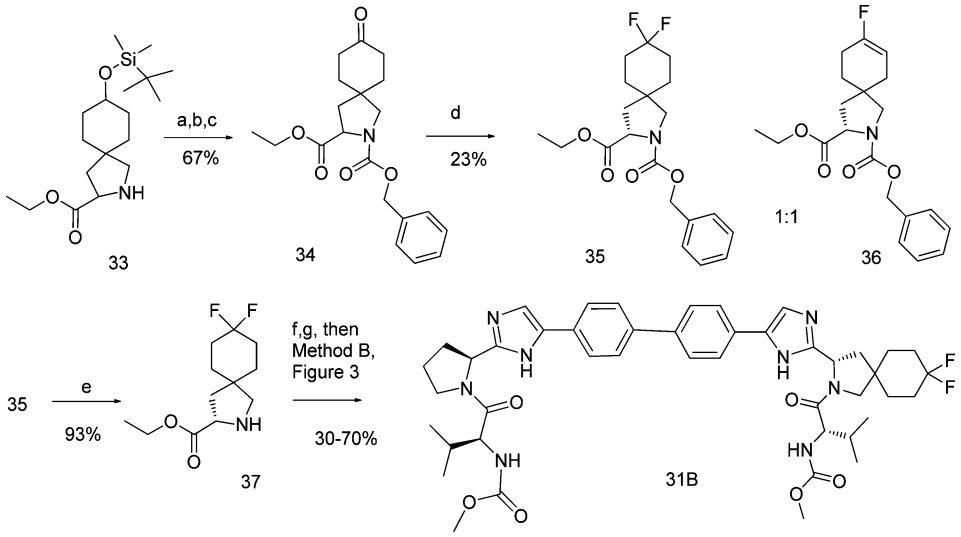

Figure 6. Synthesis of **31B**. Reagents and conditions are as follows: (a) CH_2Cl_2, CBz-Cl, Et_3N; (b) THF, TBAF, CH_3COOH; (c) CH_2Cl_2, Dess–Martin periodinane; (d) (1) Deoxo-Fluor, EtOH; (2) CH_2Cl_2, mCPBA, (3) chiral chromatography; (e) $Pd(OH)_2$, EtOH, H_2; (f) CH_2Cl_2, CM-Val, HATU, Hunig's base; (g) LiOH, THF–water–MeOH.

enantiomeric **35** to **37** was followed by chemistry described in method A (Figure 3), affording **31B** as single isomer (Figure 6). Similar chemistry afforded the difluorocyclobutane analogue **31N** as a diastereomeric mixture.

Potency data in both the four- and six-membered series (Table 3) revealed that the more polar X (SO_2, NH) in spirocycles **31A**, **31D**, and **31I** were detrimental to both gt1b and, in particular, to gt1a replicon potencies. Bulky X in **31C**, **31E**, **31F**, **31H**, **31J–M** were generally not well-tolerated. In contrast, inhibitors with small and less polar X (O, CF_2) in **31B**, **31G**, and **31N** were very potent in both assays. The influence of the spirocyclic ring size on potency was somewhat context-dependent. For X = CF_2 (**31B** and **31N**) and X = methyl carbamate (**31F** and **31K**), the six-membered ring was preferred over the four-membered ring. However, for remaining X in Table 3 (X = N-Boc for **31C** and **31H**; X = NH for **31D** and **31I**; X = N-Ac for **31E** and **31J**) the four-membered ring was preferred. The most potent inhibitor in this series, **31B**, featured a substantial potency improvement especially in the gt1a assay over the most potent 5-spiro series inhibitors **25A** and **25H**. We tested **31B** in the transient replicon gt1b NS5A mutant assays. While **31B** was equipotent against the wild type and L28V mutant, mutants L31V and Y93H caused 158- and 794-fold reductions in EC_{50} values for this compound, respectively (Table 6). We were encouraged by the improvement of potency as we progressed from the 5-spiro to the 4-spiro series and felt that further explorations in the 4-spiro series could address sensitivity of some gt1b mutants, in particular with small and nonpolar X moieties, such as oxygen or sulfur in the spirocyclic ring.

4-Spiroketal and Thioketal Inhibitors. We next designed ketal and thioketal spiropyrrolidines **41A–H** (Table 4). Intermediate **38** facilitated robust syntheses of diverse (ring size, ring substituents) 4-spirocyclic acids **40** (Figure 7), which were then elaborated into **41A-H** as described in methods A and B (Figure 3). There was no/little ring size effect on potency (**41D** and **41H**) and the X = S and X = O analogues were essentially equipotent (**41A** and **41H**), although a somewhat higher gt1a potency slightly favored **41H**. However, methyl

dx.doi.org/10.1021/jm4013104 | J. Med. Chem. 2014, 57, 2058–2073

Table 4. gt1a and gt1b Replicon Potencies of 41A–H

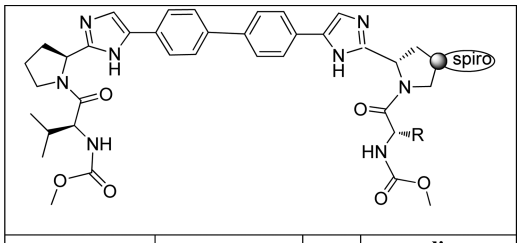

Compound	spiro	R	replicon pEC$_{50}$	
			Gt 1a	Gt 1b
41A	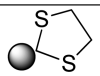	*i*-Pr	10.1	11.4
41B	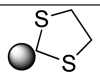	Et	10.2	11.4
41C	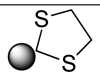	H	9.2	11.3
41D		*i*-Pr	10.6	11.1
41E		Me	10.1	10.7
41F	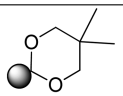	*i*-Pr	9.1	11.6
41G	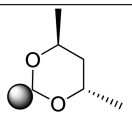	*i*-Pr	8.7	10.9
41H GSK2336805		*i*-Pr	10.4	11.1

substituents on the ketal moiety (**41F**, **41G** vs **41D**) and smaller R (**41A** and **41C**, **41D** and **41E**) were detrimental to gt1a (but not gt1b) potency. This SAR contrasts with the 5-spiro SAR, where smaller N-substituents, such as acetyl in **25A**, were associated with the potency increase. The most potent compounds in the HCV replicon assays in this series were **41B**, **41D**, and **41H**.

Within the caveats and limitations of our NS5A homology model, we considered possible interactions of **41H** bound to NS5A gt1b domain I. The model suggested that the peptidic caps of **41H** interact cooperatively and favorably with the dimer interface (Figure 8). Both peptidic caps access the cavities formed between the ZnF and N-terminal α-helix units of the dimer interface in a similar, but nonequivalent, manner, supporting a network of hydrogen bond interactions across the dimer interface. Sterically, the 4-spiro ketal pyrrolidine motif helps stabilize a network of intermonomer interactions (R30–Y93, R30–I52) at the dimer interface while orienting the carbamate terminus of **41H** to make bridging hydrogen bond interactions with the backbone NH of L31 and the side chains of R30 and T56 (Figure 8b). Conserved (gt1a/gt1b) I52 forms a steric buttress against the 4-spiroketal in supporting these interactions. Although the 4-spiroketal can in principle make a hydrogen bond contact with R30, this contact would be relatively hydrated and therefore is considered negligible. Notably, the side chain of conserved T95 is oriented to form a bridging hydrogen bond between the imidazole of the **41H** core and Q54. Similar to the 4-spiroketal motif, the des-spiro cap also helps stabilize intermonomer interactions between R30 and Y93, as well as R30 and the I52 backbone carbonyl (Figure 8c). However, here the peptidic cap is buried more deeply in the dimer cavity and the proline and carbamate carbonyls make bridging hydrogen bonds to R30 and Y93, respectively. There is no obvious hydrogen bond to the core imidazole other than the possibility of a bridging water interaction with T56. As a class, dimeric NS5A inhibitors have notably weaker gt1a potency than gt1b. Given their proximity to the putative binding mode of **41H**, gt1a/gt1b residue variations M/L28, Q/R30, H/Q54, R/T56, and H/P58 would be predicted to most sensitively modulate gt1a vs gt1b potency. For example, Q30 in gt1a would be expected to have fewer intermonomer and/or ligand interactions than in the case of R30 in gt1b, suggesting weaker stabilization of the dimer interface (and less restriction of the N-terminal α-helix).

For gt1a Y93C and gt1b Y93H resistant mutations, the model suggests that Y93 intermonomer interactions with Q/R30 would

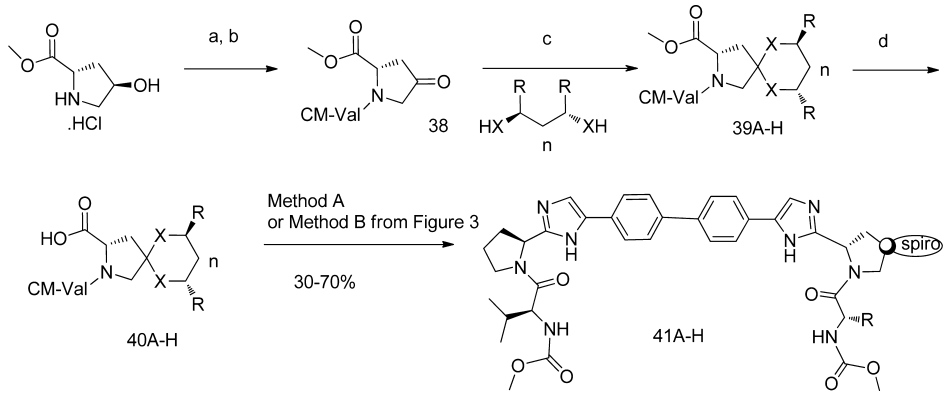

Figure 7. Synthesis of **41A–H**. Reagents and conditions are as follows: (a) HATU, Et_3N, CM-Val; (b) Dess–Martin periodinane; (c) X = S or O, tosylic acid; (d) LiOH, THF–water–MeOH.

dx.doi.org/10.1021/jm4013104 | J. Med. Chem. 2014, 57, 2058–2073

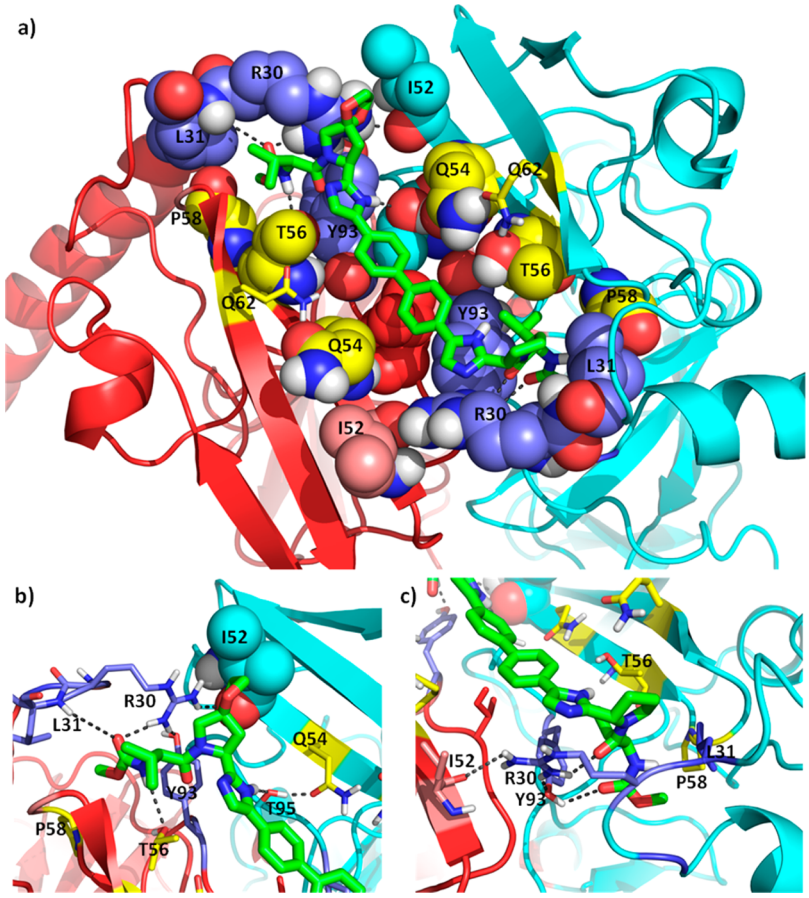

Figure 8. Putative binding mode of **41H** (sticks, green carbons) with NS5A gt1b domain I. (a) **41H** spans the homodimer interface, enabling the peptidic caps to cooperatively bind within the cavities formed between the ZnF and N-terminal α-helix units of the dimer. The NS5A monomers are color-coded red and cyan. Resistant mutation sites (gt1a, M28T, Q30H/R, L31M, Y93C; gt1b, L31V, Y93H),[7] color-coded blue, surround the peptidic caps, while differential gt1a/gt1b residues (H/Q54, R/T56, H/P58, E/Q62), color-coded yellow, flank the biaryl core along the central dimer interface. Ligand contacts are depicted as CPK spheres. (b) Magnified view of the 4-spiroketal cap binding pocket depicting ligand contacts and the hydrogen-bonding network surrounding the pocket. An intermonomer hydrogen bond between R30 and Y93 helps form the binding cavity. R30 also forms an intermonomer hydrogen bond with backbone carbonyl of conserved I52. I52 serves as a steric buttress against the 4-spiroketal, while the terminal carbamate of the cap makes bridging hydrogen bond contacts to the backbone of L31 and the side chains of R30 and T56. The T95 hydroxyl is oriented to interact with the imidazole of the biaryl core. (c) Magnified view of the des-spiro cap binding pocket. R30 again makes intermonomer hydrogen bonds with Y93 and I52. In contrast to (b), the proline and carbamate carbonyls of the cap make bridging hydrogen bonds to R30 and Y93, respectively, while there is no apparent hydrogen bond to the core imidazole.

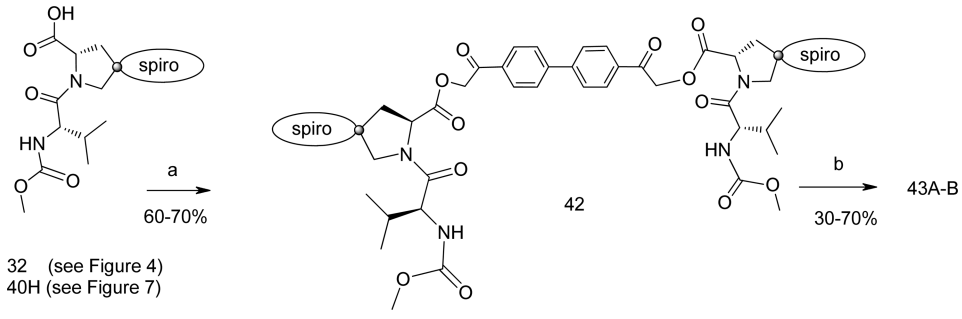

Figure 9. Synthesis of **43A**,**B**. Reagents and conditions are as follows: (a) Et_3N, CH_3CN, **14**; (b) ammonium acetate, dioxane, 110 °C, 48 h or microwave 160 °C, 20 min.

be eliminated in both cases (Figure 8b,c), effectively destabilizing the dimer interface and relaxing cavity formation. Moreover, L31V and Y93H mutants introduce residues with reduced molecular volume, and we thus speculate that the added steric bulk of the 4-spiroketal may compensate this void, establishing new intermolecular interactions that restore the potencies of **41H** and **43B** against gt1b L31V and Y93H to essentially gt1b wt level.

Symmetric 4-Spiro Inhibitors. Chiral separation of **30** enabled the synthesis of symmetric inhibitor **43A** as single isomer. Both **43A** and the symmetric ketal **43B** were synthesized from dibromide **14** and acids **32** and **40** (X = O, R = H, n = 0), respectively, followed by cyclization of diester **42** (Figure 9).

dx.doi.org/10.1021/jm4013104 | J. Med. Chem. 2014, 57, 2058−2073

Inhibitor **43A** turned out to be somewhat more potent in gt1a replicon than both nonsymmetric **41H** and symmetric **43B**. On the other hand, both the symmetric bis-ketal **43B** and nonsymmetric (mono) ketal **41H** were essentially equivalent in gt1a and gt1b replicon assays (Table 5).

Table 5. gt1a and gt1b Replicon Potencies of 43A,B

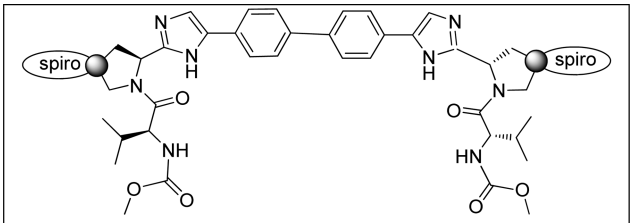

Compound	spiro	replicon pEC_{50}	
		Gt 1a	Gt 1b
43A	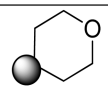	10.7	10.9
43B	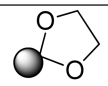	10.3	11.0

HCV NS5A gt1b Mutant Characterization and Rat Pharmacokinetics of HCV Inhibitors. Daclatasvir **6** and key inhibitors that emerged from this work, **31B**, **43A**, **43B**, and **41H**, were evaluated in the transient replicon gt1b L28V, L31V, and Y93H mutant assays (Table 6). The pEC_{50} values for all five

Table 6. Potencies (pEC_{50}) of NS5A Compounds in Transient gt1b Replicon Mutant Assay (% Fitness of Mutant vs Wild Type)

	transient replicon pEC_{50}			
compd	WT[a] gt1b (100%)	L28V (ND[b])	L31V (353%)	Y93H (56%)
6	11.3	11.4	9.9	9.5
31B	11.9	11.8	9.7	9.0
41H	11.1	11.5	10.6	10.6
43A	11.4	11.2	10.7	9.9
43B	10.9	10.9	10.6	10.9

[a]Wild type. [b]Not determined.

compounds on the L28V mutant were similar to that of wild type, suggesting that the amino acid substitution did not impact potency of the compounds. All compounds showed reduced potencies against the L31V mutant, although its impact varied significantly between compounds. Thus, the EC_{50} potencies of **6** and **31B** were reduced ≥25-fold but ≤5-fold for **43A**, **43B**, and **41H**, compared to the wild type virus. Evaluation of these five compounds on the Y93H mutant showed that **6**, **31B**, and **43A** pEC_{50} values were reduced by ≥30-fold, while for **41H** only 3.2-fold reduction was observed, compared to wild type. No change in potency was observed for **43B**. These results demonstrated that **41H** and **43B** had the best profile on the mutants, and both were thus progressed to further PK studies.

As seen in Table 7, both compounds exhibited a similar in vivo clearance (about 60% hepatic blood flow), but **41H** was

Table 7. In Vivo Pharmacokinetic Data for 41H and 43B

compd	animal species	in vivo CL as % hepatic blood flow[a]	*F*, %
43B	CD rat	58	9
41H	CD rat	60	13
	beagle dog	8	51
	cynomolgus monkey	9	13

[a]Liver blood flow (mL min^{-1} kg^{-1}): rat = 55; dog = 30; cyno = 45.

somewhat more bioavailable and was thus progressed to additional PK studies in other species. Dog and cyno PK data indicated that **41H** was a low-clearance compound in both species, with high bioavailability in dog. In the hepatocyte stability assessment, **41H** was found to be stable in dog, cynomolgus monkey, and human hepatocytes ($t_{1/2} \geq 360$ min, all three species) but, consistent with its higher rat in vivo clearance, somewhat less stable in rat hepatocytes ($t_{1/2} = 160$ min).

Inhibitor **41H** was nontoxic in cellular assays up to 40 μM. It did not inhibit cytochrome P450 enzymes 1A2, 2C9, 2D6, 2C19, and 3A4 ($IC_{50} > 33$ μM) and was inactive in the P450 3A4 time-dependent assay against midazolam, nifedipine, and atorvastatin, thus displaying a low risk for drug−drug interaction, an important factor for the anticipated combination HCV therapy. In addition, **41H** was 94% bound to human serum albumin and 86% to human α1AGP.

The ability of **41H** to reduce the level of HCV RNA in the gt1b replicon cells was evaluated over 20 days with **6** run in parallel as a comparator (Figure 10). The replicon cells were maintained in

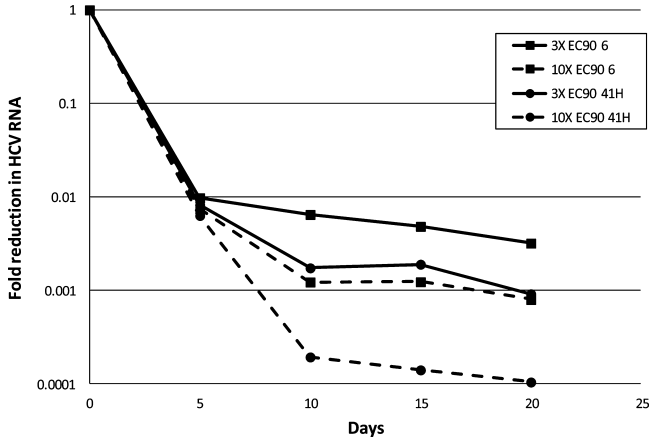

Figure 10. Inhibitors **41H** and **6** in HCV gt1b RNA reduction assay.

concentrations of **6** or **41H** that was 3 or 10 times the EC_{90} value of the compound calculated from the results in the standard 2-day assay. Initially both concentrations of **6** and **41H** caused similar declines in HCV RNA with a ~2 $\log_{10}$ reduction of HCV RNA observed at day 5. After this initial decline, compound **41H** was able to further reduce HCV RNA levels to 3 and 4 $\log_{10}$ by day 20 for the 3× and 10× EC_{90} concentrations, respectively. Compound **6** was able to cause further reduction in HCV RNA levels, but the maximum reduction was between 2 and 3 $\log_{10}$. Thus, at 10-fold over EC_{90}, **41H** was able to reduce HCV RNA levels by 10-fold more than observed for **6**. The combined data supported progressing **41H** to the clinic.

In a clinical study, **41H** demonstrated good pharmacokinetics in single and multiple ascending dose studies in healthy volunteers and was well tolerated up to 60 mg single dose and 75 mg in 14-day multiple dose study. Genotype 1 HCV infected

dx.doi.org/10.1021/jm4013104 | J. Med. Chem. 2014, 57, 2058−2073

patients were given a single dose of up to 120 mg of **41H**, and HCV viral load was monitored. Mean HCV RNA reductions from baseline ranged from 0.996 $\log_{10}$ copies/mL for patients receiving a single dose of 1 mg up to a mean reduction of 2.95 $\log_{10}$ copies/mL after a single dose of 120 mg.[35,36]

CONCLUSIONS

The clinical and preclinical results validated our medicinal chemistry strategy. Even though the 5-spiro analogues **25A** and **25H** were slightly less potent in gt1a replicon than **6**, their improved potency compared to **4** and **5** encouraged us to explore the 4-spiro series. This effort identified potent non-ketal inhibitors **31B** and **31G** and established SAR of the spiro moiety. The preference for small, relatively nonpolar X (Table 3) discovered in the 4-spiro non-ketal series directed our explorations into the ketal-based 4-spiropyrrolidines, leading to potent nonsymmetric **41H** and symmetric **43B** NS5A inhibitors. The PK data across species were consistent with further progression of **41H**. In addition to exhibiting good potency profile in the NS5A gt1b L31V and Y93H mutant assay, **41H** also reduced HCV RNA in a 20-day study to a greater degree than daclatasvir **6** (Figure 10), suggesting that it could be less impacted by gt1b-resistant mutants. Clinical data generated to date support further development of **41H**.

EXPERIMENTAL SECTION

HCV in Vitro Data. Stable HCV Replicon Data for Compounds 1−5 (Table 1). Huh-luc/neo-ET replicon cells were removed from flasks with a 0.05% trypsin/EDTA solution and resuspended in medium supplemented with 10% FBS, penicillin−streptomycin, nonessential amino acids, glutamine, and geneticin. The cell density was adjusted to 7.9×10^4 cells/mL, and an amount of 95 μL of cell suspension was placed in columns 2−12 of 96-well plates using a MultiDrop liquid dispenser (Thermo LabSystems), for a density of 7500 cells/well. Then 95 μL of medium was dispensed to column 1 for the background controls. Two sets of plates were prepared: white opaque plates for assay of luciferase activity and clear plates for assay of cytotoxicity. The cell plates were incubated overnight at 37 °C, 5% CO_2. Compound plates were prepared with 10-point, 2-fold serial dilutions of the test compounds in duplicate, with four compounds assayed per 96-well plate. An amount of 10 μL from the compound dilution plates was transferred to the cell culture plates using a multichannel pipettor or a RapidPlate 96/384 workstation (Caliper Lifesciences). The cell plates were incubated for 48 h at 37 °C, 5% CO_2. To determine luciferase activity, an amount of 100 μL of Steady-Glo reagent (Promega) was added to the culture medium, and the plates were shaken on a plate shaker. The plates were incubated for 15−30 min at room temperature, and the luminescence was read on an Analyst HT luminometer (Molecular Devices) with a 1 s integration time. To determine cytotoxicity, an amount of 10 μL of WST-detection reagent (Roche) was added to the culture medium. Plates were incubated at 37 °C, 5% CO_2, for approximately 60 min. Absorbance at 440 nm was measured using the SpectraMax Plus microplate spectrophotometer (Molecular Devices). Data analysis for the luciferase and cytotoxicity assays was performed using Graphpad Prism, version 4.0 (Graphpad Software, Inc.), in conjunction with DS Accord for EXCEL 6.0 (Accelrys, Microsoft Corp.). The percent inhibition and percent cytotoxicity values were plotted against compound concentration, and the data were fit to a constrained four-parameter sigmoidal fit, equivalent to the "four-parameter logistic equation". The curve-fit equation employed was $Y = \text{Bottom} + (\text{Top} - \text{Bottom})/[1 + (10^{(\log EC_{50} - X)^{\text{Hillslope}}})]$, where Bottom is the minimum Y value, Top is the maximum Y value, and Hillslope is the slope of the linear portion of the semilog curve. Top and Bottom were constrained to values of 100% and 0%, respectively. The minimum n (number of independent measurements) for each compound was 2. The average pEC_{50} SD in the gt1a data was less than 0.21 and in the gt1b less than 0.25. All other stable and transient HCV replicon data were obtained by the method described in ref 17 (http://dx.doi.org/10.1021/jm400317w).

Chemistry. Unless stated otherwise, the reagents were obtained from commercial sources and were used directly. Reactions involving air- or moisture-sensitive reagents were carried out under nitrogen atmosphere. The reactions were carried out at ambient temperature unless otherwise indicated. Silica gel (EM Science, 230−400 mesh) was used for chromatographic purification unless otherwise indicated. Anhydrous solvents were obtained from Aldrich (Sure Seal). ^{1}H NMR spectra were recorded on a Varian 300 or 400 MHz spectrometer. The chemical shifts are reported in parts per million (ppm) relative to TMS. The following abbreviations are used to describe peak patterns when appropriate: b, broad, s, singlet, d, doublet, t, triplet, q, quartet, m, multiplet. Mass spectra were obtained using electrospray (positive or negative ion). All compounds were >95% pure as determined by LC/MS (equipped with UV and evaporative light scattering detectors) in both acid- and base-modified CH_3CN/water gradients and ^{1}H NMR.

2-Amino-1-(4-bromophenyl)ethanone (7). To a stirred solution of 2-bromo-1-(4-bromophenyl)ethanone (130 g, 0.478 mol) in toluene (2500 mL) was added hexamethylenetetramine (65.6 g 0.478 mol), and the mixture was stirred at 40 °C for 16 h. The resulting solid was filtered off and washed with toluene and ether to give a white solid. To a stirred suspension of this solid in EtOH (800 mL) was added concentrated hydrochloride acid (300 mL). The mixture was stirred at ambient temperature for 20 h, and the solid was collected by filtration, washed with EtOH, water, and dried in vacuo to give **7** (95 g, 92%) as a white solid, used without purification in the next step. ^{1}H NMR (300 MHz, DMSO-d_6) δ ppm 8.58 (s, br, 2H), 7.96 (d, J = 8.7 Hz, 2H), 7.81 (d, J = 8.7 Hz, 2H), 4.48−4.52 (m, 2H). ES LC−MS m/z = 214, 216 $(M + H)^+$.

1,1-Dimethylethyl {2-Oxo-2-[4-(4,4,5,5-tetramethyl-1,3,2-dioxaborolan-2-yl)phenyl]ethyl}carbamate (8). To a mixture of **7** (50 g, 0.2 mol) and Boc_2O (48 g, 0.22 mol) in CH_2Cl_2 (1000 mL), TEA (68.8 mL, 0.5 mol) was added dropwise at 0 °C. The mixture was stirred at ambient temperature overnight and washed with 1 N HCl (300 mL × 3) and brine, dried over Na_2SO_4, concentrated in vacuo to give an off-white solid, which was further washed with petroleum ether and dried. $Pd(dppf)Cl_2$ (2.6 g 3.18 mmol) was added to a mixture of 1,1-dimethylethyl [2-(4-bromophenyl)-2-oxoethyl]carbamate (20 g, 63.7 mmol), bis(pinacolato)diboron (19.4 g, 76.4 mmol), and KOAc (24.8 g, 0.254 mol) in dioxane (300 mL). The flask was purged with nitrogen (3×) and heated to 80 °C for 16 h under nitrogen atmosphere. The reaction mixture was diluted with hexane (300 mL), filtered, concentrated, and the residue was purified by chromatography on silica gel (petroleum ether/ethyl acetate = 5/1) to give **8** (13.3 g, 58%) as a white solid. ^{1}H NMR (300 MHz, $CDCl_3$) δ ppm 7.90−7.93 (m, 4H), 5.55 (s, br,1H), 4.68 (s, 2H), 1.48 (s, 9H), 1.35 (s, 12H). ES LC−MS m/z = 384 $(M + Na)^+$.

1,1-Dimethylethyl (2*S*)-2-({[2-(4-Bromophenyl)-2-oxoethyl]-amino}carbonyl)-1-pyrrolidinecarboxylate, (9). A mixture of Boc-L-proline (50 g, 0.233 mol), HATU (106 g, 0.279 mol), and DIEA (150 mL) in DMF (400 mL) was stirred at ambient temperature for 10 min, followed by the addition of **7** (70 g, 0.279 mol) in DMF (500 mL). The mixture was stirred overnight, diluted with EtOAc (4 L), washed with 1 N HCl (500 mL × 4) and brine, dried over Na_2SO_4, and concentrated. The crude product was recrystallized from a mixture of petroleum ether/ethyl acetate (2/1) to give **9** (58.4 g, 61%) as a yellow solid. ^{1}H NMR (300 MHz, DMSO) δ ppm 8.22 (s, 1H), 7.93 (d, J = 8.4 Hz, 2H), 7.77 (d, J = 8.4 Hz, 2H), 4.46−4.51 (m, 2H), 4.15−4.21 (m, 1H), 3.28−3.40 (m, 2H),1.78−1.90 (m, 4H), 1.29−1.41 (m, 9H). ES LC−MS m/z = 411.1, 4113.1 $(M + H)^+$.

1,1-Dimethylethyl (2*S*)-2-[4-(4-Bromophenyl)-1*H*-imidazol-2-yl]-1-pyrrolidinecarboxylate (10). A mixture of compound **9** (40.0 g, 97.2 mmol) and NH_4OAc (60 g, 0.778 mol) in xylene (400 mL) was heated to 150 °C for 5 h. The reaction mixture was concentrated, and the residue was dissolved in EtOAc (500 mL), washed with aqueous $NaHCO_3$ and brine. The organic phase was dried over Na_2SO_4, concentrated to dryness. The crude product was purified by chromatography on silica gel (petroleum ether/ethyl acetate = 1/1) to give 1,1-dimethylethyl(2*S*)-2-[4-(4-bromophenyl)-1*H*-imidazol-2-

dx.doi.org/10.1021/jm4013104 | J. Med. Chem. 2014, 57, 2058−2073

yl]-1-pyrrolidinecarboxylate (**10**) (34 g, 89%) as a brown solid. ^{1}H NMR (300 MHz, $CDCl_3$) δ ppm 7.52 (d, J = 8.4 Hz, 2H), 7.46 (d, J = 8.4 Hz, 2H), 7.20(s, 1H), 5.58−5.71 (m, 1H), 3.38−3.42 (m, 1H), 2.80−2.87 (m, 2H), 2.03−2.06 (m, 2H), 1.88−2.00 (m, 2H), 1.49 (s, 9H). ES LC−MS m/z = 392, 394 $(M + H)^+$.

Methyl [(1*S*)-1-({(2*S*)-2-[4-(4-Bromophenyl)-1*H*-imidazol-2-yl]-1-pyrrolidinyl}carbonyl)-2-methylpropyl]carbamate (11). Compound **10** (72.4 g, 185 mmol) was treated with saturated HCl in dioxane (200 mL) and stirred at ambient temperature overnight. The resulting solid was filtered and washed with petroleum ether to give 4-(4-bromophenyl)-2-[(2*S*)-2-pyrrolidinyl]-1*H*-imidazole (60 g, 90%) as a yellow solid. ^{1}H NMR (300 MHz, DMSO-d_6) δ ppm 8.10 (s, 2H), 7.88 (d, J = 6.6 Hz,2H), 7.70 (d, J = 6.6 Hz, 2H), 7.49 (s, 1H), 7.32 (s, 1H), 7.16 (s, 1H), 4.50−4.52 (m, 1H), 3.15−3.40 (m, 2H), 1.88−2.88 (m, 4H). ES LC−MS m/z = 291.1, 293.1 $(M + H)^+$.

A mixture of *N*-[(methyloxy)carbonyl]-L-valine (prepared according to the procedure provided in patent WO2005061487) (43.1 g, 0.246 mol) and HATU (93.5 g, 0.246 mol) in CH_2Cl_2 (1000 mL) was stirred for 10 min. 4-(4-Bromophenyl)-2-[(2*S*)-2-pyrrolidinyl]-1*H*-imidazole ((60 g, 0.205 mol) was introduced, followed by DIEA (82.6 mL, 0.308 mol) dropwise. The mixture was stirred at ambient temperature for 12 h, diluted with CH_2Cl_2 (1000 mL), and washed with $NaHCO_3$ and brine. The organic phase was dried over Na_2SO_4, concentrated to dryness, and purified by chromatography (silica gel, petroleum ether/ethyl acetate = 1/1) to give **11** (62 g, 67%) as a yellow solid. ^{1}H NMR (300 MHz, $CDCl_3$) δ 7.43−7.51(m, 4H), 7.17 (s, 1H), 5.53−5.57 (m, 1H), 5.20−5.22 (m, 1H), 5.29−5.33 (m, 1H), 3.64−3.71 (m, 5H), 2.99−3.03 (m, 1H), 1.88−2.31 (m, 4H), 0.88−0.92 (m, 6H). ES LC−MS m/z = 449, 451 $(M + H)^+$.

Methyl {(1*S*)-1-[((2*S*)-2-{4-[4′-(Aminoacetyl)-4-biphenylyl]-1*H*-imidazol-2-yl}-1-pyrrolidinyl)carbonyl]-2-methylpropyl}carbamate (12). To a mixture of **11** (62 g, 0.138 mol), **8** (47.7 g, 0.152 mol), and $NaHCO_3$ (34.2 g, 0.414 mol) in a mixed DME (800 mL) and water (260 mL) was added Pd(dppf)Cl_2 (5.63 g, 6.9 mmol). The flask was purged with nitrogen (3×) before being heated to 80 °C for 16 h. The mixture was cooled to room temperature and filtered. The filtrate was diluted with EtOAc (1000 mL), washed with $NaHCO_3$, brine, dried over Na_2SO_4, and concentrated. The residue was purified by flash chromatography (silica gel, petroleum ether/ethyl acetate = 1/2) to give the Boc-protected product (45 g, 54%) as a yellow solid. ^{1}H NMR (300 MHz, $CDCl_3$) δ ppm 8.03 (d, J = 8.4 Hz, 2H), 7.88−760 (m, 6H), 5.58 (S, br,1H), 5.42 (m, 1H), 5.28−5.30 (m,1H), 4.71 (s, 2H), 4.32−4.35 (m, 1H), 3.70−3.84 (m, 5H), 2.96 (s, br,1H), 1.96−2.11 (m, 4H), 1.49 (s, 9H), 0.88−0.92 (m, 6H). ES LC−MS m/z = 604, $(M + H)^+$. A solution of the Boc-protected product (3.8 g, 6.3 mmol) in CH_2Cl_2 (40 mL) was treated with HCl (10 mL, 4 M in dioxane) to give **12** as a light yellow solid (3.5 g, quant).

(*S*)-2-(4′-(2-Bromoacetyl)-[1,1′-biphenyl]-4-yl)-2-oxoethyl-1-((*S*)-2-((methoxycarbonyl)amino)-3-methylbutanoyl)-pyrrolidine-2-carboxylate (16). 1,1′-(4,4′-Biphenyldiyl)bis(2-bromoethanone) (37.8 g, 95 mmol) was dissolved in DMF (800 mL) and degassed for 15 min (N_2). **15** (21.99 g, 81 mmol) was dissolved in DMF (100 mL), followed by careful addition of NaH (2.94 g, 73.4 mmol, 60% in oil) under nitrogen over 15 min, then slowly added over 15 min dropwise to a solution of 1,1′-(4,4′-biphenyldiyl)bis(2-bromoethanone), followed by stirring for 1 h at room temperature. Solvent volume was then reduced in vacuo to ∼100 mL and cooled to 20 °C. An amount of 100 mL of water was slowly added, and resulting slight gray-yellow solid was filtered, washed with water (200 mL), hexane (200 mL), and dried under the vacuum (12h). The crude compound was purified on 500 g of silica with hexane/ethyl acetate (increasing gradient from 50% to 100% EA), yielding 14.5 g (37.3%) of compound **16**. ^{1}H NMR (400 MHz, DMSO-d_6) δ ppm 8.11 (dd, J = 12.0, 8.5 Hz, 4 H), 7.96 (d, J = 8.4 Hz, 4 H), 7.41 (d, J = 8.4 Hz, 1 H), 5.43−5.75 (m, 2 H), 4.99 (s, 2 H), 4.53 (dd, J = 8.6, 4.7 Hz, 1 H), 4.03 (t, J = 8.6 Hz, 1 H), 3.76−3.90 (m, 1 H), 3.60−3.73 (m, 1 H), 3.53 (s, 3 H), 2.22−2.37 (m, 1 H), 2.12−2.21 (m, 1 H), 1.85−2.06 (m, 3 H), 0.90 (dd, J = 10.7, 6.6 Hz, 6 H).

For the preparation of target compounds **25A−H**/**31A−N** and **41A−H**, the corresponding acid components were utilzied in the following two methods to provide the final compounds.

Method A. To a stirred solution of carboxylic acid component (0.25 mmol) in DMF (2 mL) were added TEA (0.77 mmol) and HATU (0.28 mmol). After the mixture was stirred for ∼3 min, the amine **12** (0.25 mmol) was introduced. After the mixture was stirred for an additional 2 h at room temperature, the mixture was directly loaded to RP HPLC column, eluting with 5−80% CH_3CN/water (0.2% NH_3H_2O (conc)) to give the corresponding amide as an intermediate. To a stirred solution of the amides (0.15 mmol) in dioxane (3 mL) was added ammonium acetate (1.57 mmol). The mixture was heated to 110 °C in a sealed tube overnight, cooled to room temperature, filtered to remove excess ammonium acetate, and purified by column chromatography (silica gel, 0−15% MeOH in ethyl acetate) to give the final target compounds (as an example **25A**) as a solid.

Method B. **16** (95 mmol) was dissolved in DMF (800 mL) and degassed for 15 min (N_2). Acid component **15** (21.99 g, 81 mmol) was dissolved in DMF (100 mL), followed by careful addition of NaH (2.94 g, 73.4 mmol, 60% in oil) under nitrogen over 15 min, then slowly added over 15 min dropwise to a DMF solution of bromo compound followed by stirring for 1 h at room temperature. Solvent volume was then reduced in vacuo to ∼100 mL and cooled to 20 °C. An amount of 100 mL of water was slowly added, and the resulting slight gray-yellow solid was filtered, washed with water (200 mL), hexane (200 mL), and dried under the vacuum (12 h). The crude compound was purified on 500 g of silica with hexane/ethyl acetate (increasing gradient from 50% to 100% EA), yielding 30−70% of the final target compounds.

Ethyl 2-[(Diphenylmethylidene)amino]-4-(tetrahydro-4*H*-pyran-4-ylidene)butanoate (18). To a solution of ethyl 2-(diphenylmethyleneamino)acetate (5.29 g, 19.8 mmol), benzyltriethylammonium chloride (0.41 g, 1.8 mmol), and cesium hydroxide monohydrate (4.54 g, 27.0 mmol) in anhydrous CH_2Cl_2 (50 mL) was added 4-(2-bromoethylidene)tetrahydro-2*H*-pyran (3.44 g, 18.0 mmol) in anhydrous CH_2Cl_2 (40 mL). The mixture was stirred at room temperature for 72 h under nitrogen. The mixture was partitioned between CH_2Cl_2 and water, and the aqueous layer was extracted with CH_2Cl_2. The organic layer was dried over Na_2SO_4 and concentrated in vacuo. The residue was purified by silica gel chromatography, eluting with 5−40% hexanes/EtOAc to afford the title compound as a clear oil in quantitative yield.

Ethyl 2-Amino-4-(tetrahydro-4*H*-pyran-4-ylidene)butanoate (19). To a solution of **18** (6.8 g, 18.0 mmol) in THF (30 mL) were added water (30 mL) and glacial acetic acid (20 mL), and the mixture was stirred at room temperature for 2.5 h. The mixture was concentrated in vacuo and the residue dissolved in 0.1 N HCl. It was extracted twice with ethyl acetate, and the organic layer was discarded. To the aqueous layer was added solid K_2CO_3 until the solution gave blue pH paper. The aqueous layer was extracted with 15% isopropanol/CH_2Cl_2 (3×) and the organic layer dried over Na_2SO_4 and concentrated in vacuo to afford the title compound as a clear oil (3.05 g, 79%).

Ethyl 2-{[(4-Nitrophenyl)sulfonyl]amino}-4-(tetrahydro-4*H*-pyran-4-ylidene)butanoate (20). To a solution of **19** (1.0 g, 4.7 mmol) in anhydrous CH_2Cl_2 (30 mL) was added Hunig's base (1.6 mL, 9.4 mmol) followed by 4-nitrobenzenesulfonyl chloride (1.14 g, 5.2 mmol), and the mixture was stirred at room temperature under nitrogen for 2 h. The mixture was diluted with CH_2Cl_2 and washed with 0.1 N HCl. The organic layer was dried over $MgSO_4$ and concentrated in vacuo. The residue was purified by silica gel chromatography, eluting with 10−70% hexanes/EtOAc to afford the title compound as an off-white solid in quantitative yield.

Ethyl 1-[(4-Nitrophenyl)sulfonyl]-8-oxa-1-azaspiro[4.5]-decane-2-carboxylate (21). To a solution of **20** (1.87 g, 4.7 mmol) in anhydrous chloroform (47 mL) was added trifluoromethanesulfonic acid (0.2 mL, 2.3 mmol), and the mixture was stirred at room temperature under nitrogen for 4 h. The mixture was diluted with CH_2Cl_2 and washed with saturated $NaHCO_3$ and the organic layer dried over $MgSO_4$ and concentrated in vacuo. The residue was purified by silica gel chromatography, eluting with 10−70% hexanes/EtOAc to afford the title compound as a white solid (1.47 g, 79%). ^{1}H NMR (400 MHz, $CDCl_3$) δ ppm 8.19−8.36 (m, 2 H), 8.08 (d, J = 8.8 Hz, 2 H), 4.52 (dd, J = 8.5, 2.1 Hz, 1 H), 3.99−4.14 (m, 2 H), 3.87−3.99 (m, 2 H), 3.21−3.49 (m, 2 H), 2.58−2.78 (m, 2 H), 2.10−2.30 (m, 2 H), 1.89−

dx.doi.org/10.1021/jm4013104 | J. Med. Chem. 2014, 57, 2058−2073

2.06 (m, 2 H), 1.77 (dd, J = 13.0, 2.1 Hz, 1 H), 1.35 (dd, J = 12.9, 1.6 Hz, 1 H), 1.22 (t, J = 7.1 Hz, 3 H). LC−MS ESI $(M + H)^+$ = 399.47.

Ethyl 8-Oxa-1-azaspiro[4.5]decane-2-carboxylate (22). To a solution of **21** (1.47 g, 3.7 mmol) in anhydrous CH_3CN (25 mL) were added K_2CO_3 (0.76 g, 5.5 mmol), 18-crown-6 (0.2 g, 0.7 mmol), and thiophenol (0.6 mL. 5.5 mmol), and the mixture was stirred at room temperature for 18 h. The mixture was concentrated in vacuo and the residue dissolved in 0.1 N HCl. The aqueous layer was extracted twice with EtOAc, and the organic layer was discarded. The aqueous layer was treated with solid K_2CO_3 until the solution gave blue pH paper. It was extracted with 15% isopropanol/CH_2Cl_2 (3×) and the organic layer dried over Na_2SO_4 and concentrated in vacuo to afford the title compound as a clear oil (0.71 g, 90%).

1-{*N*-[(Methyloxy)carbonyl]-L-valyl}-8-oxa-1-azaspiro[4.5]-decane-2-carboxylic Acid (23). To a solution of **22** (125 mg, 0.59 mmol) in anhydrous CH_2Cl_2 (2 mL) was added silver cyanide (98 mg, 0.73 mmol) followed by *N*-[(methyloxy)carbonyl]-L-valyl chloride (142 mg, 0.73 mmol) as a solution in anhydrous CH_2Cl_2 (3.5 mL), and the solution was stirred at room temperature for 18 h under nitrogen. The mixture was filtered and treated with MeOH and stirred for 5 min. The mixture was concentrated in vacuo and the residue purified by silica gel chromatography, eluting with 30−100% hexanes/EtOAc to afford the ester intermediate as a white solid (43 mg, 20%).

To a solution of the above ester (80 mg, 0.2 mmol) in THF/water/MeOH (1.0 mL/0.5 mL/0.5 mL) was added lithium hydroxide monohydrate (13 mg, 0.3 mmol), and the mixture was stirred at room temperature for 72 h. The mixture was treated with 1 N HCl (0.5 mL) and the mixture partitioned between EtOAc and 0.1 N HCl. The organic layer was separated and dried over $MgSO_4$ and concentrated in vacuo to afford the title compound **23** as a white solid (53 mg, 72%). ^{1}H NMR (400 MHz, DMSO-d_6) δ ppm 12.88 (br s, 1 H), 7.45−7.61 (m, 1 H), 4.89−5.03 (m, 1 H), 3.70−3.87 (m, 2 H), 3.65 (t, J = 9.2 Hz, 1 H), 3.53 (s, 3 H), 3.02 (td, J = 12.9, 4.9 Hz, 1 H), 2.71−2.90 (m, 1 H), 2.22−2.38 (m, 1 H), 1.87−2.19 (m, 3 H), 1.53−1.73 (m, 1 H), 1.32−1.42 (m, 1 H), 1.06−1.15 (m, 1 H), 0.61−0.98 (m, 8 H). LC−MS ESI $(M + H)^+$ = 342.95.

1-Acetyl-8-oxa-1-azaspiro[4.5]decane-2-carboxylic Acid (24). To a solution of **22** (135 mg, 0.63 mmol) in anhydrous CH_2Cl_2 (2 mL) was added Hunig's base (0.22 mL, 1.3 mmol) followed by acetyl chloride (0.05 mL, 0.76 mmol), and the mixture was stirred at room temperature under nitrogen for 1.5 h. The mixture was diluted with CH_2Cl_2 and washed with 0.1 N HCl and the organic layer dried over $MgSO_4$ and concentrated in vacuo. The residue was purified by silica gel chromatography, eluting with 60−100% hexanes/EtOAc to afford the acetyl compound as a yellow oil (94 mg, 58%). To a solution of this ester (93 mg, 0.34 mmol) in THF/water/MeOH (1.1 mL/0.6 mL/0.6 mL) was added lithium hydroxide monohydrate (29 mg, 0.69 mmol), and the mixture was stirred at room temperature for 3 h. The mixture was treated with 1 N HCl (0.7 mL) and partitioned between EtOAc and 0.1 N HCl. The aqueous layer was extracted twice with EtOAc, and the combined organic layers were dried over $MgSO_4$ and concentrated in vacuo to afford the title compound **24** as a white solid (79 mg, 95%).

Methyl ((1*S*)-1-{[(2*S*)-2-(4-{4′-[2-(1-Acetyl-8-oxa-1-azaspiro-[4.5]dec-2-yl)-1*H*-imidazol-4-yl]-4-biphenylyl}-1*H*-imidazol-2-yl)-1-pyrrolidinyl]carbonyl}-2-methylpropyl)carbamate (25A). Yield, 19 mg, 17%. ^{1}H NMR (400 MHz, MeOH-d_4) δ ppm 7.51−7.90 (m, 8 H), 7.17−7.52 (m, 2 H), 5.08−5.26 (m, 2 H), 3.81−4.03 (m, 4 H), 3.64 (s, 3 H), 3.41−3.61 (m, 3 H), 2.21−2.51 (m, 5 H), 2.01−2.21 (m, 4 H), 1.97 (d, J = 19.9 Hz, 5 H), 1.77−1.91 (m, 1 H), 1.64−1.75 (m, 1 H), 1.31−1.42 (m, 1 H), 0.79−1.04 (m, 8 H). HRMS for $C_{39}H_{48}N_7O_5$ $(M + H)^+$ calcd, 694.3717; found, 694.3718.

Methyl ((1*S*)-1-{[(2*S*)-2-(4-{4′-[2-(1-Acetyl-8,8-difluoro-1-azaspiro[4.5]dec-2-yl)-1*H*-imidazol-4-yl]-4-biphenylyl}-1*H*-imidazol-2-yl)-1-pyrrolidinyl]carbonyl}-2-methylpropyl)-carbamate (25B). ^{1}H NMR (400 mHz, $CDCl_3$) δ 11.17−10.07 (m, 2 H), 8.16−7.40 (m, 10 H), 7.35−7.03 (m, 2 H), 5.85−4.98 (m, 2 H), 4.59−4.12 (m, 1 H), 3.72 (s, 5 H), 3.46 (br s, 1 H), 3.33−2.72 (m, 2 H), 2.76−1.39 (m, 17 H), 1.27−0.74 (m, 5 H). HRMS for $C_{40}H_{48}F_2N_7O_4$ $(M + H)^+$ calcd, 728.3736; found, 728.3736.

Benzyl 2-(5-(4′-(2-((*S*)-1-((*S*)-2-((Methoxycarbonyl)amino)-3-methylbutanoyl)pyrrolidin-2-yl)-1*H*-imidazol-5-yl)-[1,1′-biphenyl]-4-yl)-1*H*-imidazol-2-yl)-8-oxa-1-azaspiro[4.5]decane-1-carboxylate (25C). ^{1}H NMR (400 MHz, MeOH-d_4) δ ppm 8.17 (br s, 1 H), 7.80 (d, J = 8.21 Hz, 1 H), 7.64−7.77 (m, 9 H), 7.28−7.40 (m, 3 H), 7.13 (br s, 2 H), 6.98 (d, J = 8.40 Hz, 2 H), 5.13−5.22 (m, 2 H), 4.15−4.26 (m, 1 H), 3.86−4.01 (m, 4 H), 3.64 (s, 3 H), 3.43−3.60 (m, 3 H), 3.01−3.19 (m, 1 H), 2.77 (br s, 1 H), 2.27−2.39 (m, 4 H), 2.12−2.26 (m, 2 H), 2.02−2.08 (m, 3 H), 1.71 (br s, 1 H), 1.44 (br s, 1 H), 0.95−1.02 (m, 1 H), 0.91 (dd, J = 17.10, 6.74 Hz, 6 H).

Methyl [(1*S*)-2-Methyl-1-({(2*S*)-2-[4-(4′-{2-[1-((2*S*)-3-methyl-2-{[(methyloxy)carbonyl]amino}butanoyl)-8,8-dioxido-8-thia-1-azaspiro[4.5]dec-2-yl]-1*H*-imidazol-4-yl}-4-biphenylyl)-1*H*-imidazol-2-yl]-1-pyrrolidinyl}carbonyl)propyl]carbamate (25D). ^{1}H NMR (400 mHz, $CDCl_3$) δ 7.92−7.52 (m, 9 H), 5.39 (br s, 4 H), 4.36 (br s, 1 H), 3.98−3.82 (m, 1 H), 3.82−3.60 (m, 10 H), 3.19 (br s, 4 H), 2.88−2.70 (m, 1 H), 2.33 (br s, 4 H), 2.02 (s, 4 H), 1.81 (br s, 5 H), 1.06 (s, 1 H), 0.89 (d, J = 7.0 Hz, 6 H), 0.74 (d, J = 6.5 Hz, 3 H), 0.44−0.34 (m, 3 H). HRMS for $C_{44}H_{57}N_8O_8S$ $(M + H)^+$ calcd, 857.4020; found, 857.4018.

Methyl [(1*S*)-2-Methyl-1-({(2*S*)-2-[4-(4′-{2-[1-((2*S*)-3-methyl-2-{[(methyloxy)carbonyl]amino}butanoyl)-8-oxa-1-azaspiro-[4.5]dec-2-yl]-1*H*-imidazol-4-yl}-4-biphenylyl)-1*H*-imidazol-2-yl]-1-pyrrolidinyl}carbonyl)propyl]carbamate (25E). ^{1}H NMR (400 MHz, MeOH-d_4) δ ppm 7.56−7.86 (m, 9 H), 7.16−7.44 (m, 2 H), 6.88−7.09 (m, 1 H), 5.72 (br s, 1 H), 5.09−5.21 (m, 1 H), 4.03−4.28 (m, 1 H), 3.80−4.04 (m, 6 H), 3.42−3.71 (m, 9 H), 2.11−2.56 (m, 8 H), 1.88−2.11 (m, 6 H), 0.80−1.06 (m, 12 H). HRMS for $C_{44}H_{57}N_8O_7$ $(M + H)^+$ calcd, 809.4350; found, 809.4347.

Methyl [(1*S*)-1-({(2*S*)-2-[4-(4′-{2-[8,8-Difluoro-1-((2*S*)-3-methyl-2-{[(methyloxy)carbonyl]amino}butanoyl)-1-azaspiro[4.5]-dec-2-yl]-1*H*-imidazol-4-yl}-4-biphenylyl)-1*H*-imidazol-2-yl]-1-pyrrolidinyl}carbonyl)-2-methylpropyl]carbamate (25F). ^{1}H NMR (400 mHz, MeOH-d_4) δ 7.92−7.51 (m, 8 H), 7.29 (br s, 2 H), 5.71 (br s, 1 H), 5.32 (br s, 1 H), 4.21 (d, J = 7.4 Hz, 1 H), 4.15−3.80 (m, 4 H), 3.77−3.41 (m, 8 H), 3.18 (br s, 1 H), 3.12−2.82 (m, 1 H), 2.63−1.40 (m, 16 H), 1.05−0.84 (m, 10 H), 0.78−0.64 (m, 1 H), 0.44−0.28 (m, 1 H). HRMS for $C_{45}H_{57}F_2N_8O_6$ $(M + H)^+$ calcd, 843.4369; found, 843.4368.

Methyl [(1*S*)-1-({8,8-Difluoro-2-[4-(4′-{2-[(2*S*)-1-((2*S*)-3-methyl-2-{[(methyloxy)carbonyl]amino}butanoyl)-2-pyrrolidinyl]-1*H*-imidazol-4-yl}-4-biphenylyl)-1*H*-imidazol-2-yl]-1-azaspiro-[4.5]dec-1-yl}carbonyl)propyl]carbamate (25G). ^{1}H NMR (400 mHz, $CDCl_3$) δ 7.84 (d, J = 7.8 Hz, 3 H), 7.72−7.41 (m, 6 H), 7.31−7.09 (m, 3 H), 5.73−5.17 (m, 4 H), 5.12 (br s, 1 H), 4.41−4.06 (m, 3 H), 3.97−3.56 (m, 11 H), 3.37−2.76 (m, 4 H), 2.60−1.55 (m, 9 H), 1.46−1.20 (m, 2 H), 1.06 (d, J = 6.0 Hz, 2 H), 1.00−0.79 (m, 5 H), 0.56 (d, J = 7.3 Hz, 1 H). HRMS for $C_{44}H_{55}F_2N_8O_6$ $(M + H)^+$ calcd, 829.4213; found, 829.4211.

Methyl ((1*S*)-2-{8,8-Difluoro-2-[4-(4′-{2-[(2*S*)-1-((2*S*)-3-methyl-2-{[(methyloxy)carbonyl]amino}butanoyl)-2-pyrrolidinyl]-1*H*-imidazol-4-yl}-4-biphenylyl)-1*H*-imidazol-2-yl]-1-azaspiro-[4.5]dec-1-yl}-1-methyl-2-oxoethyl)carbamate (25H). ^{1}H NMR (400 mHz, $CDCl_3$) δ 10.97−10.14 (m, 2 H), 7.91−7.40 (m, 8 H), 7.34−7.16 (m, 2 H), 5.68−5.15 (m, 3 H), 5.08 (d, J = 6.0 Hz, 1 H), 4.34 (d, J = 8.0 Hz, 2 H), 3.95−3.54 (m, 8 H), 3.37−2.69 (m, 4 H), 2.60−1.57 (m, 13 H), 1.56−1.18 (m, 3 H), 1.06 (d, J = 6.8 Hz, 1 H), 0.89 (d, J = 6.5 Hz, 6 H). HRMS for $C_{43}H_{53}F_2N_8O_6$ $(M + H)^+$ calcd, 815.4056; found, 815.4061.

Methyl [(1*S*)-1-({8,8-Difluoro-2-[4-(4′-{2-[(2*S*)-1-((2*S*)-3-methyl-2-{[(methyloxy)carbonyl]amino}butanoyl)-2-pyrrolidinyl]-1*H*-imidazol-4-yl}-4-biphenylyl)-1*H*-imidazol-2-yl]-1-azaspiro-[4.5]dec-1-yl}carbonyl)-3-methylbutyl]carbamate (25I). ^{1}H NMR (400 mHz, $CDCl_3$) δ 11.07−9.94 (m, 2 H), 8.17−7.42 (m, 10 H), 7.33−7.08 (m, 2 H), 5.72−5.19 (m, 3 H), 5.14−4.99 (m, 1 H), 4.86 (br s, 1 H), 4.50−4.09 (m, 2 H), 4.02−3.50 (m, 8 H), 3.45 (s, 1 H), 3.33−2.71 (m, 4 H), 2.59−1.47 (m, 11 H), 1.40 (br s, 3 H), 1.19−0.67 (m, 11 H), 0.63−0.40 (m, 1 H).). HRMS for $C_{46}H_{59}F_2N_8O_6$ $(M + H)^+$ calcd, 857.4526; found, 857.4531.

2-{*N*-[(Methyloxy)carbonyl]-L-valyl}-8-oxa-2-azaspiro[4.5]-decane-3-carboxylic Acid (32). To a solution of **30** (200 mg, 0.94 mmol), HATU (392 mg, 1.03 mmol), and *N*-[(methyloxy)carbonyl]-L-

dx.doi.org/10.1021/jm4013104 | J. Med. Chem. 2014, 57, 2058−2073

valine (181 mg, 1.03 mmol) in anhydrous CH_2Cl_2 (6 mL) was added Hunig's base (0.33 mL, 1.88 mmol), and the solution was stirred at room temperature under nitrogen. After 2 h, the mixture was concentrated in vacuo and purified by C_{18} RP chromatography, eluting with 10−90% ACN/water/0.2% NH_4OH to afford the ester as a yellow oil (313 mg, 90%). To a solution of this ester (310 mg, 0.84 mmol) in a 2:1:1 mixture of THF/water/MeOH (6 mL) was added lithium hydroxide monohydrate (70 mg, 1.67 mmol), and the mixture was stirred at room temperature for 2 h. The mixture was treated with 1 N HCl (1.6 mL), partitioned between EtOAc and water (30 mL each), and the organic layer was extracted with EtOAc (30 mL), dried ($MgSO_4$), and concentrated to give **32** as a white foam (211 mg, 74%). This material was used in subsequent steps without additional purification. ^{1}H NMR (400 MHz, DMSO-d_6) δ ppm 12.43 (br s, 1 H), 7.19−7.41 (m, 1 H), 4.05−4.28 (m, 1 H), 3.91−4.05 (m, 2 H), 3.40−3.71 (m, 6 H), 3.20−3.28 (m, 1 H), 1.81−1.98 (m, 2 H), 1.70−1.80 (m, 1 H), 1.46−1.69 (m, 2 H), 1.32−1.46 (m, 1 H), 0.65−1.03 (m, 10 H).

3-Ethyl 2-(Phenylmethyl)-8-oxo-2-azaspiro[4.5]decane-2,3-dicarboxylate (34). To a solution of ethyl **33** (10.61 g, 31.3 mmol) dissolved in dry CH_2Cl_2 was added Et_3N (10.8 mL, 78 mmol). The mixture was cooled to 0 °C followed by the addition of Cbz-Cl (6.2 mL, 43.5 mmol), and the mixture was stirred at 0 °C for 5 min at room temperature for 1 h. The mixture was diluted with CH_2Cl_2 (700 mL), washed with 0.1 N HCl (700 mL), dried ($MgSO_4$), and concentrated in vacuo. The residue was purified by silica gel chromatography, eluting with 10−60% hexanes/EtOAc to afford the cbz protected compound as a yellow oil (5.73 g, 39%). To a solution of this intermediate (5.73 g, 12.05 mmol) in THF (60 mL) was added glacial acetic acid (1.38 mL, 24.0 mmol) followed by TBAF (24 mL) as a 1 M solution in THF. The mixture was stirred at room temperature for 72 h. The mixture was partitioned between EtOAc and water (250 mL) each. The organic layer was separated and washed with saturated $NaHCO_3$ (100 mL) and dried ($MgSO_4$) and concentrated in vacuo. The reaction was found to be incomplete by TLC. The residue was dissolved in dry THF (60 mL), cooled to 0 °C, and treated with HF−pyridine (1.6 mL, 18.0 mmol), warmed to room temperature, and stirred for 2 h under nitrogen. The mixture was poured into saturated $NaHCO_3$ (100 mL), and solid K_2CO_3 was added until gas evolution ceased. Extraction was with EtOAc (2 × 150 mL). The organic layers were combined and washed with 0.1 N HCl (100 mL), dried ($MgSO_4$), and concentrated in vacuo to afford the title compound in quantitative yield as a yellow oil which was used in subsequent reactions without additional purification. To a solution of the intermediate from above (4.36 g, 120.05 mmol) in dry CH_2Cl_2 (60 mL) was added Dess−Martin periodinane (10.22 g, 24.1 mmol), and the mixture was stirred at room temperature under nitrogen for 18 h. The mixture was poured into 10% aqueous sodium thiosulfate (150 mL) and saturated $NaHCO_3$ (150 mL) and stirred for 10 min. Extraction was with CH_2Cl_2 (2 × 150 mL). The mixture was dried ($MgSO_4$) and concentrated in vacuo. The residue was purified by silica gel chromatography, eluting with 25−80% hexanes/EtOAc to afford **34** as a pale yellow oil (2.89 g, 67%).

3-Ethyl 2-(Phenylmethyl)-(3*S*)-8,8-difluoro-2-azaspiro[4.5]-decane-2,3-dicarboxylate (35). To a solution of **34** (2.89 g, 7.13 mmol) in anhydrous CH_2Cl_2 (50 mL) was added Deoxo-Fluor (2.2 mL, 12.1 mmol) followed by a catalytic amount of EtOH, and the mixture was stirred at room temperature under nitrogen. After 2.5 h the mixture was poured into saturated $NaHCO_3$ (150 mL) and stirred for 10 min. Extraction was with CH_2Cl_2 (2 × 150 mL), and the organic layer was washed with 0.1 N HCl (100 mL), dried ($MgSO_4$), and concentrated in vacuo to afford the desired compound (as a racemic mixture) as a yellow oil (3.01 g) which was found to be contaminated with **36** in a 1:1 ratio. The residue was dissolved in dry CH_2Cl_2 (35 mL) and treated with mCPBA (77%, 1.66 g, 7.45 mmol) and stirred under nitrogen for 18 h. The mixture was poured into saturated $NaHCO_3$ (40 mL) and 10% aqueous sodium thiosulfate (40 mL) and stirred for 10 min. Extraction was with CH_2Cl_2 (100 mL). The mixture was dried ($MgSO_4$) and concentrated in vacuo. The residue was purified by silica gel chromatography, eluting with 5−50% hexanes/EtOAc. The racemate was then separated by chiral HPLC on a 10 μm o.d. column, eluting with 25% isopropanol in hexanes to afford the title compound as a clear oil (632 mg, 23%). The absolute configurations were determined by vibrational circular dichroism (VCD). ^{1}H NMR (400 MHz, $CDCl_3$) δ ppm 7.28−7.41 (m, 5 H), 4.98−5.23 (m, 2 H), 4.37 (ddd, J = 19.3, 8.1, 8.0 Hz, 1 H), 4.22 (q, J = 7.2 Hz, 1 H), 3.93−4.12 (m, 1 H), 3.45−3.70 (m, 1 H), 3.36 (dd, J = 10.8, 2.0 Hz, 1 H), 2.22 (dd, J = 12.8, 8.5 Hz, 1 H), 1.79−2.03 (m, 4 H), 1.59−1.78 (m, 4 H), 1.56 (br s, 1 H), 1.28 (t, J = 7.1 Hz, 1 H), 1.22 (d, J = 6.1 Hz, 1 H), 1.13 (t, J = 7.1 Hz, 1 H). LC−MS ESI $(M + H)^+$ = 381.68.

Ethyl (3*S*)-8,8-Difluoro-2-azaspiro[4.5]decane-3-carboxylate (37). To **35** (630 mg, 1.65 mmol) in absolute EtOH (12 mL) was added 20% $Pd(OH)_2$ on carbon (65 mg), and the mixture was hydrogenated on a Fisher-Porter apparatus for 18 h at 60 psi. The mixture was filtered through Celite and concentrated in vacuo to afford the title compound as a clear oil (380 mg, 93%).

(3*S*)-8,8-Difluoro-2-{*N*-[(methyloxy)carbonyl]-L-valyl}-2-azaspiro[4.5]decane-3-carboxylic Acid. To a solution of **37** (380 mg, 1.54 mmol) in anhydrous CH_2Cl_2 (10 mL) were added HATU (614 mg, 1.6 mmol), *N*-[(methyloxy)carbonyl]-L-valine (283 mg, 1.6 mmol) followed by Et_3N (0.43 mL, 3.1 mmol), and the mixture was stirred at room temperature under nitrogen for 1 h. The mixture was concentrated in vacuo and the residue purified by silica gel chromatography, eluting with 15−80% hexanes/EtOAc. Appropriate fractions were combined and concentrated in vacuo. The residue was dissolved in THF/water/MeOH (5 mL/2.5 mL/2.5 mL), and lithium hydroxide monohydrate was added (119 mg, 2.8 mmol). The solution was stirred at room temperature for 30 min. The mixture was treated with 1 N HCl (3.5 mL) and partitioned between EtOAc and water (50 mL each). The aqueous layer was extracted with ethyl acetate (50 mL). The organic layers were combined and dried ($MgSO_4$) and concentrated in vacuo. The residue was triturated in diethyl ether and concentrated in vacuo to afford the title compound as a white solid (542 mg, 93%). ^{1}H NMR (400 MHz, DMSO-d_6) δ ppm 12.47 (br s, 1 H), 7.41 (d, J = 8.0 Hz, 1 H), 4.24 (t, J = 8.6 Hz, 1 H), 3.95−4.14 (m, 2 H), 3.52 (s, 3 H), 3.25−3.33 (m, 1 H), 2.22 (dd, J = 12.3, 8.4 Hz, 1 H), 1.79−2.11 (m, 5 H), 1.58−1.77 (m, 3 H), 1.41−1.59 (m, 2 H), 0.93 (dd, J = 12.7, 6.6 Hz, 6 H). LC−MS ESI $(M + H)^+$ = 377.23. Method B was utilized for the synthesis of **31B**.

Methyl [(1*S*)-2-Methyl-1-({(2*S*)-2-[4-(4′-{2-[2-((2*S*)-3-methyl-2-{[(methyloxy)carbonyl]amino}butanoyl)-8,8-dioxido-8-thia-2-azaspiro[4.5]dec-3-yl]-1*H*-imidazol-4-yl}-4-biphenylyl)-1*H*-imidazol-2-yl]-1-pyrrolidinyl}carbonyl)propyl]carbamate (31A). ^{1}H NMR (400 MHz, MeOH-d_4) δ ppm 7.64 (br s, 10 H), 7.32 (br s, 2 H), 5.05−5.24 (m, 1 H), 4.04−4.29 (m, 1 H), 3.99 (br s, 1 H), 3.81 (br s, 1 H), 3.55−3.73 (m, 6 H), 3.03−3.25 (m, 4 H), 1.80−2.47 (m, 14 H), 0.68−1.06 (m, 16 H). HRMS for $C_{44}H_{57}N_8O_8S$ $(M + H)^+$ calcd, 857.4020; found, 857.4020.

Methyl [(1*S*)-1-({(2*S*)-2-[4-(4′-{2-[8,8-Difluoro-2-((2*S*)-3-methyl-2-{[(methyloxy)carbonyl]amino}butanoyl)-2-azaspiro[4.5]-dec-3-yl]-1*H*-imidazol-4-yl}-4-biphenylyl)-1*H*-imidazol-2-yl]-1-pyrrolidinyl}carbonyl)-2-methylpropyl]carbamate (31B). ^{1}H NMR (400 MHz, MeOH-d_4) δ ppm 7.69−7.82 (m, 3 H), 7.63 (br s, 5 H), 7.17−7.37 (m, 2 H), 5.03−5.19 (m, 1 H), 4.20 (br s, 1 H), 4.06−4.16 (m, 1 H), 3.96 (br s, 1 H), 3.85 (br s, 1 H), 3.62 (d, J = 3.1 Hz, 6 H), 2.24−2.38 (m, 3 H), 2.15 (br s, 3 H), 1.85−2.09 (m, 8 H), 1.77−1.85 (m, 2 H), 1.53−1.76 (m, 3 H), 0.96 (br s, 4 H), 0.87 (d, J = 6.3 Hz, 12 H). HRMS for $C_{45}H_{57}N_8O_6F_2$ $(M + H)^+$ calcd, 843.4369; found, 843.4371.

1,1-Dimethylethyl 2-{*N*-[(Methyloxy)carbonyl]-L-valyl}-3-(4-{4′-[2-((2*S*)-1-{*N*-[(methyloxy)carbonyl]-L-valyl}-2-pyrrolidinyl)-1*H*-imidazol-4-yl]-4-biphenylyl}-1*H*-imidazol-2-yl)-2,8-diazaspiro[4.5]decane-8-carboxylate (31C). ^{1}H NMR (400 MHz, MeOH-d_4) δ ppm 7.56−7.87 (m, 10 H), 7.31 (br s, 2 H), 5.04−5.23 (m, 1 H), 4.11−4.32 (m, 2 H), 3.93−4.04 (m, 1 H), 3.80−3.92 (m, 1 H), 3.63 (s, 6 H), 3.33−3.61 (m, 6 H), 1.86−2.49 (m, 9 H), 1.68 (br s, 1 H), 1.56 (br s, 2 H), 1.37−1.49 (m, 9 H), 0.81−1.08 (m, 15 H). HRMS for $C_{49}H_{65}N_9O_8$ $(M + H)^+$ calcd, 908.5034; found, 908.5031.

Methyl [(1*S*)-2-Methyl-1-({(2*S*)-2-[4-(4′-{2-[2-((2*S*)-3-methyl-2-{[(methyloxy)carbonyl]amino}butanoyl)-2,8-diazaspiro[4.5]-dec-3-yl]-1*H*-imidazol-4-yl}-4-biphenylyl)-1*H*-imidazol-2-yl]-1-pyrrolidinyl}carbonyl)propyl]carbamate (31D). ^{1}H NMR (400 MHz, MeOH-d_4) δ ppm 7.56−7.83 (m, 10 H), 7.31 (br s, 2 H), 5.00−5.22 (m, 2 H), 4.12−4.30 (m, 3 H), 4.01 (br s, 1 H), 3.80−3.91 (m, 1 H),

dx.doi.org/10.1021/jm4013104 | J. Med. Chem. 2014, 57, 2058−2073

3.57−3.70 (m, 6 H), 2.76−3.07 (m, 4 H), 1.89−2.48 (m, 10 H), 1.69−1.81 (m, 1 H), 1.61 (br s, 2 H), 0.82−1.09 (m, 15 H). HRMS for $C_{44}H_{58}N_9O_6$ (M + H)$^+$ calcd, 808.4510; found, 808.4509.

Methyl [(1*S*)-1-({(2*S*)-2-[4-(4′-{2-[8-Acetyl-2-((2*S*)-3-methyl-2-{[(methyloxy)carbonyl]amino}butanoyl)-2,8-diazaspiro[4.5]dec-3-yl]-1*H*-imidazol-4-yl}-4-biphenylyl)-1*H*-imidazol-2-yl]-1-pyrrolidinyl}carbonyl)-2-methylpropyl]carbamate (31E). ^{1}H NMR (400 MHz, MeOH-d_4) δ ppm 7.54−7.88 (m, 10 H), 7.32 (br s, 2 H), 5.05−5.23 (m, 2 H), 4.03−4.34 (m, 2 H), 3.71−4.03 (m, 3 H), 3.56−3.71 (m, 8 H), 3.34−3.56 (m, 2 H), 2.14−2.46 (m, 4 H), 1.89−2.14 (m, 6 H), 1.46−1.83 (m, 4 H), 1.19−1.32 (m, 2 H), 0.78−1.07 (m, 14 H). HRMS for $C_{46}H_{60}N_9O_7$ (M + H)$^+$ calcd, 850.4616; found, 850.4617.

Methyl 2-{*N*-[(Methyloxy)carbonyl]-L-valyl}-3-(4-{4′-[2-((2*S*)-1-{*N*-[(methyloxy)carbonyl]-L-valyl}-2-pyrrolidinyl)-1*H*-imidazol-4-yl]-4-biphenylyl}-1*H*-imidazol-2-yl)-2,8-diazaspiro[4.5]decane-8-carboxylate (31F). ^{1}H NMR (400 MHz, MeOH-d_4) δ ppm 7.51−7.92 (m, 10 H), 7.32 (br s, 2 H), 5.02−5.25 (m, 1 H), 4.03−4.31 (m, 2 H), 3.75−4.05 (m, 2 H), 3.61−3.72 (m, 7 H), 3.34−3.60 (m, 4 H), 1.82−2.50 (m, 7 H), 1.70 (br s, 2 H), 1.44−1.63 (m, 4 H), 1.27 (br s, 4 H), 0.77−1.10 (m, 14 H). HRMS for $C_{46}H_{60}N_9O_8$ (M + H)$^+$ calcd, 866.4565; found, 850.4564.

Methyl [(1*S*)-2-Methyl-1-({(2*S*)-2-[4-(4′-{2-[2-((2*S*)-3-methyl-2-{[(methyloxy)carbonyl]amino}butanoyl)-8-oxa-2-azaspiro[4.5]dec-3-yl]-1*H*-imidazol-4-yl}-4-biphenylyl)-1*H*-imidazol-2-yl]-1-pyrrolidinyl}carbonyl)propyl]carbamate (31G). ^{1}H NMR (400 MHz, MeOH-d_4) δ ppm 7.55−7.87 (m, 8 H), 7.32 (br s, 4 H), 5.02−5.23 (m, 3 H), 4.13−4.34 (m, 4 H), 3.93−4.04 (m, 1 H), 3.88 (br s, 2 H), 3.49−3.84 (m, 8 H), 1.86−2.54 (m, 10 H), 1.45−1.84 (m, 4 H), 0.69−1.12 (m, 12 H). HRMS for $C_{44}H_{57}N_8O_7$ (M + H)$^+$ calcd, 809.4350; found, 809.4346.

1,1-Dimethylethyl 6-{*N*-[(Methyloxy)carbonyl]-L-valyl}-7-(4-{4′-[2-((2*S*)-1-{*N*-[(methyloxy)carbonyl]-L-valyl}-2-pyrrolidinyl)-1*H*-imidazol-4-yl]-4-biphenylyl}-1*H*-imidazol-2-yl)-2,6-diazaspiro[3.4]octane-2-carboxylate (31H). Pale yellow solid (315 mg, 80%). ^{1}H NMR (400 MHz, DMSO-d_6) δ ppm 11.63−12.35 (m, 1 H), 7.47−7.92 (m, 9 H), 7.19−7.42 (m, 1 H), 5.08 (br s, 2 H), 3.94−4.23 (m, 4 H), 3.62−3.93 (m, 7 H), 3.56 (s, 6 H), 2.24−2.45 (m, 2 H), 2.14 (br s, 2 H), 1.77−2.07 (m, 6 H), 1.37 (d, J = 5.5 Hz, 9 H), 0.76−1.02 (m, 12 H). HRMS for $C_{47}H_{62}N_9O_8$ (M + H)$^+$ calcd, 880.4721; found, 880.4725.

Methyl [(1*S*)-2-Methyl-1-({(2*S*)-2-[4-(4′-{2-[6-((2*S*)-3-methyl-2-{[(methyloxy)carbonyl]amino}butanoyl)-2,6-diazaspiro[3.4]oct-7-yl]-1*H*-imidazol-4-yl}-4-biphenylyl)-1*H*-imidazol-2-yl]-1-pyrrolidinyl}carbonyl)propyl]carbamate (31I). ^{1}H NMR (400 MHz, MeOH-d_4) δ ppm 7.43−7.86 (m, 8 H), 7.04−7.42 (m, 2 H), 5.20−5.41 (m, 1 H), 5.01−5.19 (m, 2 H), 4.30−4.43 (m, 1 H), 4.12−4.27 (m, 3 H), 3.78−4.03 (m, 5 H), 3.65−3.78 (m, 4 H), 3.61−3.64 (m, 6 H), 3.39−3.52 (m, 1 H), 2.54−2.77 (m, 1 H), 2.38−2.54 (m, 1 H), 2.09−2.39 (m, 2 H), 1.89−2.13 (m, 4 H), 0.81−1.13 (m, 12 H). HRMS for $C_{42}H_{54}N_9O_6$ (M + H)$^+$ calcd, 780.4197; found, 780.4200.

Methyl [(1*S*)-1-({(2*S*)-2-[4-(4′-{2-[2-Acetyl-6-((2*S*)-3-methyl-2-{[(methyloxy)carbonyl]amino}butanoyl)-2,6-diazaspiro[3.4]oct-7-yl]-1*H*-imidazol-4-yl}-4-biphenylyl)-1*H*-imidazol-2-yl]-1-pyrrolidinyl}carbonyl)-2-methylpropyl]carbamate (31J). ^{1}H NMR (400 MHz, DMSO-d_6) δ ppm 11.67−12.33 (m, 1 H), 7.19−7.99 (m, 12 H), 5.07 (br s, 1 H), 3.92−4.25 (m, 4 H), 3.67−3.94 (m, 4 H), 3.45−3.66 (m, 8 H), 2.20−2.46 (m, 3 H), 2.17 (br s, 2 H), 1.80−2.06 (m, 5 H), 1.60−1.82 (m, 3 H), 0.78−1.02 (m, 12 H). HRMS for $C_{44}H_{56}N_9O_7$ (M + H)$^+$ calcd, 822.4303; found, 822.4300.

Methyl 6-{*N*-[(Methyloxy)carbonyl]-L-valyl}-7-(4-{4′-[2-((2*S*)-1-{*N*-[(methyloxy)carbonyl]-L-valyl}-2-pyrrolidinyl)-1*H*-imidazol-4-yl]-4-biphenylyl}-1*H*-imidazol-2-yl)-2,6-diazaspiro[3.4]octane-2-carboxylate (31K). ^{1}H NMR (400 MHz, DMSO-d_6) δ ppm 11.38−12.37 (m, 1 H), 7.58−7.93 (m, 8 H), 7.19−7.59 (m, 3 H), 4.93−5.17 (m, 1 H), 3.63−4.22 (m, 7 H), 3.45−3.64 (m, 6 H), 2.24−2.48 (m, 4 H), 2.08 (br s, 4 H), 1.79−2.07 (m, 6 H), 0.99−1.18 (m, 1 H), 0.75−0.97 (m, 14 H). HRMS for $C_{44}H_{56}N_9O_8$ (M + H)$^+$ calcd, 838.4252; found, 838.4252.

Methyl [(1*S*)-2-Methyl-1-({(2*S*)-2-[4-(4′-{2-[2-[(methylamino)carbonyl]-6-((2*S*)-3-methyl-2-{[(methyloxy)carbonyl]amino}-butanoyl)-2,6-diazaspiro[3.4]oct-7-yl]-1*H*-imidazol-4-yl}-4-biphenylyl)-1*H*-imidazol-2-yl]-1-pyrrolidinyl}carbonyl)propyl]-carbamate (31L). ^{1}H NMR (400 MHz, MeOH-d_4) δ ppm 7.64 (br s, 10 H), 7.33 (br s, 2 H), 5.06−5.22 (m, 1 H), 4.03−4.46 (m, 3 H), 3.73−4.04 (m, 8 H), 3.54−3.73 (m, 6 H), 3.46 (q, J = 7.0 Hz, 2 H), 2.52−2.76 (m, 5 H), 2.10−2.53 (m, 4 H), 2.02 (br s, 3 H), 0.70−1.09 (m, 12 H). HRMS for $C_{44}H_{57}N_{10}O_7$ (M + H)$^+$ calcd, 837.4412; found, 838.4416.

Methyl [(1*S*)-2-Methyl-1-({(2*S*)-2-[4-(4′-{2-[6-((2*S*)-3-methyl-2-{[(methyloxy)carbonyl]amino}butanoyl)-2-(methylsulfonyl)-2,6-diazaspiro[3.4]oct-7-yl]-1*H*-imidazol-4-yl}-4-biphenylyl)-1*H*-imidazol-2-yl]-1-pyrrolidinyl}carbonyl)propyl]carbamate (31M). ^{1}H NMR (400 MHz, MeOH-d_4) δ ppm 7.50−7.86 (m, 10 H), 7.33 (br s, 2 H), 5.06−5.21 (m, 1 H), 4.04−4.26 (m, 2 H), 3.75−4.05 (m, 6 H), 3.56−3.72 (m, 6 H), 3.38−3.55 (m, 2 H), 2.84−3.04 (m, 3 H), 2.70−2.86 (m, 1 H), 2.40−2.64 (m, 1 H), 2.10−2.40 (m, 3 H), 1.83−2.09 (m, 2 H), 1.20−1.37 (m, 2 H), 1.07−1.20 (m, 2 H), 0.81−1.07 (m, 12 H). HRMS for $C_{43}H_{56}N_9O_8S$ (M + H)$^+$ calcd, 858.3973; found, 858.3975.

Methyl [(1*S*)-1-({(2*S*)-2-[4-(4′-{2-[(7*S*)-2,2-Difluoro-6-((2*S*)-3-methyl-2-{[(methyloxy)carbonyl]amino}butanoyl)-6-azaspiro[3.4]oct-7-yl]-1*H*-imidazol-4-yl}-4-biphenylyl)-1*H*-imidazol-2-yl]-1-pyrrolidinyl}carbonyl)-2-methylpropyl]carbamate (31N). ^{1}H NMR (400 MHz, DMSO-d_6) δ ppm 11.42−12.37 (m, 2 H), 7.56−7.90 (m, 8 H), 7.51 (s, 2 H), 7.19−7.46 (m, 2 H), 4.73−5.39 (m, 2 H), 3.91−4.23 (m, 3 H), 3.82 (br s, 2 H), 3.54 (s, 6 H), 2.55−2.86 (m, 4 H), 2.20−2.45 (m, 2 H), 2.14 (br s, 2 H), 1.73−2.09 (m, 5 H), 0.57−0.99 (m, 12 H). HRMS for $C_{43}H_{53}N_8O_6F_2$ (M + H)$^+$ calcd, 815.4056; found, 815.4059.

Intermediates **38**, **39A−H**, **40A−H** and products **41A−H** were synthesized as previously described.[28]

Methyl [(1*S*)-2-Methyl-1-({(2*S*)-2-[4-(4′-{2-[(8*S*)-7-((2*S*)-3-methyl-2-{[(methyloxy)carbonyl]amino}butanoyl)-1,4-dithia-7-azaspiro[4.4]non-8-yl]-1*H*-imidazol-4-yl}-4-biphenylyl)-1*H*-imidazol-2-yl]-1-pyrrolidinyl}carbonyl)propyl]carbamate (41A). ^{1}H NMR (400 MHz, $CDCl_3$) δ ppm 10.07−11.08 (m, 2 H), 7.82 (br s, 3 H), 7.58 (d, J = 6.02 Hz, 5 H), 7.10−7.30 (m, 2 H), 5.54 (d, J = 9.29 Hz, 2 H), 5.17−5.42 (m, 3 H), 4.01−4.48 (m, 2 H), 3.23−4.03 (m, 10 H), 2.70−3.19 (m, 2 H), 2.30−2.49 (m, 1 H), 1.91−2.29 (m, 4 H), 1.19−1.56 (m, 4 H), 1.07 (dd, J = 10.54, 7.03 Hz, 2 H), 0.58−0.97 (m, 10 H). HRMS (M + H)$^+$ calcd, 829.3530; found, 829.3534.

Methyl [(1*S*)-2-Methyl-1-({(2*S*)-2-[4-(4′-{2-[(8*S*)-7-((2*S*)-2-{[(methyloxy)carbonyl]amino}butanoyl)-1,4-dithia-7-azaspiro[4.4]non-8-yl]-1*H*-imidazol-4-yl}-4-biphenylyl)-1*H*-imidazol-2-yl]-1-pyrrolidinyl}carbonyl)propyl]carbamate (41B). ^{1}H NMR (400 MHz, $CDCl_3$) δ ppm 9.99−11.64 (m, 2 H), 7.53 (br s, 8 H), 7.12−7.34 (m, 2 H), 5.26 (br s, 2 H), 3.18−4.64 (m, 17 H), 2.79 (br s, 2 H), 1.43−2.62 (m, 8 H), 0.70−1.19 (m, 9 H). HRMS (M + H)$^+$ calcd, 815.3373; found, 815.3373.

Methyl [(1*S*)-2-Methyl-1-({(2*S*)-2-[4-(4′-{2-[(8*S*)-7-({[(methyloxy)carbonyl]amino}acetyl)-1,4-dithia-7-azaspiro[4.4]non-8-yl]-1*H*-imidazol-4-yl}-4-biphenylyl)-1*H*-imidazol-2-yl]-1-pyrrolidinyl}carbonyl)propyl]carbamate (41C). ^{1}H NMR (400 MHz, $CDCl_3$) δ ppm 9.86−11.31 (m, 2 H), 7.50 (br s, 8 H), 6.91−7.27 (m, 2 H), 5.41−6.31 (m, 2 H), 5.24 (br s, 2 H), 3.12−4.45 (m, 18 H), 2.77 (br s, 2 H), 1.77−2.50 (m, 4 H), 0.58−1.15 (m, 6 H). HRMS (M + H)$^+$ calcd, 787.3055; found, 787.3056.

Methyl [(1*S*)-2-Methyl-1-({(2*S*)-2-[4-(4′-{2-[(3*S*)-2-((2*S*)-3-methyl-2-{[(methyloxy)carbonyl]amino}butanoyl)-6,10-dioxa-2-azaspiro[4.5]dec-3-yl]-1*H*-imidazol-4-yl}-4-biphenylyl)-1*H*-imidazol-2-yl]-1-pyrrolidinyl}carbonyl)propyl]carbamate (41D). ^{1}H NMR (400 MHz, $CDCl_3$) δ ppm 10.20−11.06 (m, 2 H), 7.35−8.02 (m, 8 H), 7.22 (d, J = 7.78 Hz, 2 H), 4.97−5.89 (m, 4 H), 3.22−4.58 (m, 15 H), 2.83−3.20 (m, 1 H), 2.58−2.83 (m, 1 H), 2.29−2.58 (m, 1 H), 1.57−2.31 (m, 8 H), 0.64−1.22 (m, 12 H). HRMS (M + H)$^+$ calcd, 811.4143; found, 811.4142.

Methyl ((1*S*)-1-Methyl-2-{(3*S*)-3-[4-(4′-{2-[(2*S*)-1-((2*S*)-3-methyl-2-{[(methyloxy)carbonyl]amino}butanoyl)-2-pyrrolidinyl]-1*H*-imidazol-4-yl}-4-biphenylyl)-1*H*-imidazol-2-yl]-6,10-dioxa-2-azaspiro[4.5]dec-2-yl}-2-oxoethyl)carbamate (41E). ^{1}H NMR (400 MHz, $CDCl_3$) δ ppm 10.04−11.11 (m, 2 H), 7.37−8.02 (m, 8 H), 7.18−7.36 (m, 2 H), 5.60 (br s, 2 H), 5.17−5.40 (m, 2 H), 3.17−4.73 (m, 14 H), 2.79−3.19 (m, 1 H), 2.45−2.81 (m, 1 H), 2.29−2.45

dx.doi.org/10.1021/jm4013104 | J. Med. Chem. 2014, 57, 2058−2073

(m, 1 H), 1.49−2.29 (m, 8 H), 1.22−1.47 (m, 3 H), 0.73−1.16 (m, 6 H). HRMS (M + H)$^+$ calcd, 783.3830; found, 783.3832.

Methyl [(1*S*)-1-({(2*S*)-2-[4-(4′-{2-[(3*S*)-8,8-Dimethyl-2-((2*S*)-3-methyl-2-{[(methyloxy)carbonyl]amino}butanoyl)-6,10-dioxa-2-azaspiro[4.5]dec-3-yl]-1*H*-imidazol-4-yl}-4-biphenylyl)-1*H*-imidazol-2-yl]-1-pyrrolidinyl}carbonyl)-2-methylpropyl]-carbamate (41F). ^{1}H NMR (400 MHz, DMSO-d_6) δ (ppm) 11.84 (br s, 1 H), 11.80 (br s, 1H), 7.90−7.60 (br m, 9H), 7.52 (s, 1H), 7.36−7.25 (br m, 2H), 5.09 (br m, 1H), 4.98 (m, 1H), 4.49 (br m, 1H), 4.14−4.02 (br m, 2H), 3.81 (br, 2H), 3.73−3.40 (br m, 11H), 2.65 (m, 1H), 2.43−2.09 (br m, 3H), 2.07−1.81 (br m, 4H), 1.05−0.75 (br m, 18H). ES LC−MS m/z = 839 (M + H)$^+$.

Methyl [(1*S*)-1-({(2*S*)-2-[4-(4′-{2-[(3*S*,7*S*,9*S*)-7,9-Dimethyl-2-((2*S*)-3-methyl-2-{[(methyloxy)carbonyl]amino}butanoyl)-6,10-dioxa-2-azaspiro[4.5]dec-3-yl]-1*H*-imidazol-4-yl}-4-biphenylyl)-1*H*-imidazol-2-yl]-1-pyrrolidinyl}carbonyl)-2-methylpropyl]carbamate (41G). ^{1}HNMR (400 MHz, $CDCl_3$) δ ppm 10.23−11.01 (m, 1 H), 7.31−8.08 (m, 8 H), 7.23 (d, J = 8.03 Hz, 2 H), 5.13−5.89 (m, 4 H), 3.34−4.69 (m, 13 H), 2.84−3.31 (m, 2 H), 2.63−2.84 (m, 1 H), 2.29−2.53 (m, 1 H), 1.85−2.29 (m, 4 H), 1.56−1.85 (m, 4 H), 1.16−1.47 (m, 6 H), 0.63−1.16 (m, 12 H). HRMS (M + H)$^+$ calcd, 835.4456; found, 835.4458.

Methyl [(1*S*)-2-Methyl-1-({(2*S*)-2-[4-(4′-{2-[(8*S*)-7-((2*S*)-3-methyl-2-{[(methyloxy)carbonyl]amino}butanoyl)-1,4-dioxa-7-azaspiro[4.4]non-8-yl]-1*H*-imidazol-4-yl}-4-biphenylyl)-1*H*-imidazol-2-yl]-1-pyrrolidinyl}carbonyl)propyl]carbamate (41H). ^{1}H NMR (400 MHz, $CDCl_3$) δ ppm 10.00−11.36 (m, 2 H), 7.56 (br s, 10 H), 7.02−7.34 (m, 2 H), 5.05−5.89 (m, 4 H), 3.76−4.65 (m, 6 H), 3.53−3.83 (m, 6 H), 2.77−3.54 (m, 2 H), 2.26−2.70 (m, 2 H), 1.45−2.26 (m, 6 H), 0.61−1.25 (m, 12 H). HRMS (M + H)$^+$ calcd, 797.3986; found, 797.3981.

Acids **32** and **40** were synthesized as previously described.[28]

Step A. To a solution of **14** (0.39 mmol) and the carboxylic acid component (0.86 mmol) in anhydrous CH_3CN (4 mL) was added Et_3N (0.19 mL, 1.4 mmol), and the solution was stirred at room temperature under nitrogen for 3.5 h. The mixture was partitioned between EtOAc and 0.1 N HCl (40 mL each). The organic layer washed with brine and dried ($MgSO_4$) and concentrated in vacuo. The residue was purified by silica gel chromatography, eluting with 20−100% hexanes/EtOAc to afford the diester product (yield 60−70%).

Step B. A mixture of diesters (97.2 mmol) and NH_4OAc (0.778 mol) in dioxane (50 mL) was heated to 160 °C for 20 min in the microwave reactor. The reaction mixture was concentrated and residue dissolved in EtOAc (500 mL) and washed with aqueous $NaHCO_3$ and brine. The organic phase was dried over Na_2SO_4 and concentrated to dryness. The crude product was purified by chromatography on silica gel (petroleum ether/ethyl acetate = 1/1) to give the product as a brown solid.

Dimethyl (4,4′-Biphenyldiylbis{1*H*-imidazole-4,2-diyl(3*S*)-8-oxa-2-azaspiro[4.5]decane-3,2-diyl[(2*S*)-3-methyl-1-oxo-1,2-butanediyl]})biscarbamate (43A). ^{1}H NMR (400 MHz, MeOH-d_4) δ ppm 7.60−7.79 (m, 10 H), 7.33 (s, 2 H), 5.11 (dd, J = 9.9, 7.9 Hz, 2H), 4.30 (d, J = 10.2 Hz, 2 H), 4.17 (d, J = 8.2 Hz, 2 H), 3.70−3.87 (m, 6 H), 3.56−3.71 (m, 10 H), 2.40 (dd, J = 12.9, 7.8 Hz, 2 H), 2.13 (dd, J = 12.6, 10.3 Hz, 2H), 1.88−2.00 (m, 2H), 1.70−1.84 (m, 4H), 1.46−1.69 (m, 6 H), 0.83−0.97 (m, 12 H). HRMS for $C_{48}H_{63}N_8O_8$ (M + H)$^+$ calcd, 879.4769; found, 879.4769.

Dimethyl (4,4′-Biphenyldiylbis{1*H*-imidazole-4,2-diyl(8*S*)-1,4-dioxa-7-azaspiro[4.4]nonane-8,7-diyl[(2*S*)-3-methyl-1-oxo-1,2-butanediyl]})biscarbamate (43B). ^{1}H NMR (400 MHz, $CDCl_3$) δ ppm 11.10−11.23 (m, 1 H), 10.10−11.63 (m, 2 H), 7.40−8.15 (m, 8 H), 7.27−7.40 (m, 2 H), 5.23−5.88 (m, 2 H), 4.31 (dd, J = 8.7, 6.5 Hz, 2 H), 3.83−4.21 (m, 10 H), 3.57−3.83 (m, 6 H), 3.05−3.46 (m, 3 H), 2.47 (dd, J = 13.5, 8.6 Hz, 2 H), 1.51−2.20 (m, 2 H), 1.08 (d, J = 6.8 Hz, 2H), 0.60−0.97 (m, 12H). HRMS (M + H)$^+$ calcd, 855.4041; found, 855.4039.

AUTHOR INFORMATION

Corresponding Author

*Phone: 919-483-9462. E-mail: wieslaw.m.kazmierski@gsk.com.

Present Address

†M.D.: HD Biosciences (China) Co., Ltd., Shanghai, China.

Notes

All authors are current or former employees of GlaxoSmithKline. The authors declare no competing financial interest.

ACKNOWLEDGMENTS

We thank all members of the program team, especially Luz H. Kryn for replicon screening, Amy Wang for virological characterization of compounds, Joel Cooper, Robert McFadyen, and Aniko Redman for expert chemistry support, and Andrew Spaltenstein and Zhi Hong for encouragement and supporting this work.

ABBREVIATIONS USED

HCV, hepatitis C virus; gt1a, genotype 1a; gt1b, genotype 1b; NS5A, nonstructural protein 5A; CM, carboxymethyl; wt, wild type

REFERENCES

(1) Alter, M. J. Epidemiology of hepatitis C virus infection. *World J. Gastroenterol.* **2007**, *13*, 2436−2441.

(2) Kamal, S. M.; Fouly, A. E.; Kamel, R. R.; Hockenjos, B.; Al Tawil, A.; Khalifa, K. E.; He, Q.; Koziel, M. J.; El Naggar, K. M.; Rasenack, J.; Afdhal, N. H. Peginterferon alfa-2b therapy in acute hepatitis C: impact of onset of therapy on sustained virologic response. *Gastroenterology* **2006**, *130*, 632−638.

(3) Tong, M. J.; El-Farra, N. S.; Reikes, A. R.; Co, R. L. Clinical outcomes after transfusion-associated hepatitis C. *N. Engl. J. Med.* **1995**, *332*, 1463−1466.

(4) Adeel, A. B.; Fasiha, K. Boceprevir and telaprevir in the management of hepatitis C virus-infected patients. *Clin. Infect. Dis.* **2012**, *54*, 96−104.

(5) Lemon, S. M.; McKeating, J. A.; Pietschmann, T.; Frick, D. N.; Glenn, J. S.; Tellinghuisen, T. L.; Symons, J.; Furman, P. A. Development of novel therapies for hepatitis C. *Antiviral Res.* **2010**, *86*, 79−92.

(6) Poenisch, M.; Bartenschlager, R. New insights into structure and replication of the hepatitis C virus and clinical implications. *Semin. Liver Dis.* **2010**, *30*, 333−347.

(7) Gao, M.; Nettles, R. E.; Belema, M.; Snyder, L. B.; Nguyen, V. N.; Fridell, R. A.; Serrano-Wu, M. H.; Langley, D. R.; Sun, J.-H.; O'Boyle, D. R., II; Lemm, J. A.; Wang, C.; Knipe, J. O.; Chien, C.; Colonno, R. J.; Grasela, D. M.; Meanwell, N. A.; Hamann, L. G. Chemical genetics strategy identifies an HCV NS5A inhibitor with a potent clinical effect. *Nature* **2010**, *465*, 96−100.

(8) Fridell, R. A.; Qiu, D.; Wang, C.; Valera, L.; Gao, M. Resistance analysis of the hepatitis C virus NS5A inhibitor BMS-790052 in an in vitro replicon system. *Antimicrob. Agents Chemother.* **2010**, *54*, 3641−3650.

(9) Lemm, J. A.; Leet, J. E.; O'Boyle, D. R.; Romine, J. L.; Huang, X. S.; Schroeder, D. R.; Alberts, J.; Cantone, J. L.; Sun, J. H; Nower, P. T.; Martin, S. W.; Serrano-Wu, M. H.; Meanwell, N. A.; Snyder, L. B.; Gao, M. Discovery of potent hepatitis C virus NS5A inhibitors with dimeric structures. *Antimicrob. Agents Chemother.* **2011**, *55*, 3795−3802.

(10) Romine, J. L.; St. Laurent, D. R.; Leet, J. E.; Martin, S. W.; Serrano-Wu, M. H.; Yang, F.; Gao, M.; O'Boyle, D. R.; Lemm, J. A.; Sun, J.-H.; Nower, P. T.; Huang, X.; Deshpande, M. S.; Meanwell, N. A.; Snyder, L. B. Inhibitors of HCV NS5A: from iminothiazolidinones to symmetrical stilbenes. *ACS Med. Chem. Lett.* **2011**, *2*, 224−229.

(11) Lopez, O. D.; Nguyen, V. N.; St. Laurent, D. R.; Belema, M.; Serrano-Wu, M. H.; Goodrich, J. T.; Yang, F.; Qiu, Y.; Ripka, A. S.; Nower, P. T.; Valera, L.; Liu, M.; O'Boyle, D. R.; Sun, J. H.; Fridell, R. A.; Lemm, J. A.; Gao, M.; Good, A. C.; Meanwell, N. A.; Snyder, L. B. HCV NS5A replication complex inhibitors. Part 3: Discovery of potent

analogs with distinct core topologies. *Bioorg. Med. Chem. Lett.* **2013**, *23*, 779−784.
(12) St Laurent, D. R; Belema, M.; Gao, M.; Goodrich, J.; Kakarla, R.; Knipe, J. O; Lemm, J. A; Liu, M.; Lopez, O. D; Nguyen, V. N; Nower, P. T.; O'Boyle, D.; Qiu, Y.; Romine, J. L.; Serrano-Wu, M. H.; Sun, J. H.; Valera, L.; Yang, F.; Yang, X.; Meanwell, N. A.; Snyder, L. B. HCV NS5A replication complex inhibitors. Part 2: Investigation of stilbene prolinamides. *Bioorg. Med. Chem. Lett.* **2012**, *22*, 6063−6.
(13) Schmitz, U.; Tan, S.-L. NS5A—from obscurity to new target for HCV therapy. Recent patents on anti-infective. *Drug Discovery* **2008**, *3*, 77−92.
(14) Cordek, D. G.; Bechtel, J. T.; Maynard, A. T.; Kazmierski, W. M.; Cameron, C. E. Targeting the protein NS5A protein of HCV: an emerging option. *Drugs Future* **2011**, *36*, 691−711.
(15) Hamatake, R.; Maynard, A.; Kazmierski, W. M. HCV Inhibition mediated through the nonstructural protein 5A (NS5A) replication complex. *Annu. Rep. Med. Chem.* **2012**, *47*, 331−345.
(16) Schmitz, F. U.; Roberts, C. D.; Abadi, A. D. M.; Griffith, R. C.; Leivers, M. R.; Slobodov, I.; Rai, R. N-Heterocyclylpyrrolidine carboxamide derivatives, processes for preparing them, pharmaceutical compositions containing them, and their use as antiviral agents. WO 2007/070600, 2006.
(17) Maynard, A.; Crosby, R. M.; Ellis, B.; Hamatake, R.; Hong, Z.; Johns, B. A.; Kahler, K. M.; Koble, C.; Leivers, A.; Leivers, M. R.; Mathis, A.; Peat, A. J.; Pouliot, J. J.; Roberts, C. D.; Samano, V.; Schmidt, R. M.; Smith, G. K.; Spaltenstein, A.; Stewart; E. L.; Thommes, P.; Turner, E. M.; Voitenleitner, C.; Walker, J. T.; Waitt, G.; Weatherhead, J.; Weaver, K.; Williams, S.; Wright, L.; Xiong, Z. Z.; Haigh, D.; Shotwell, J. B. Discovery of a potent boronic acid derived inhibitor of the HCV RNA-dependent RNA polymerase. *J. Med. Chem.* **2013**, DOI: 10.1021/jm400317w.
(18) Leivers, M. R.; Schmitz, F. U.; Griffith, R. C.; Roberts, C. D.; Dehghani Mohammad Abadi, A.; Chan, S. A.; Rai, R.; Slobodov, I.; Ton, T. L. Preparation of thiazolidine derivatives as antiviral agents. WO 2008/064218, 2007.
(19) Schmitz, F. U.; Rai, R.; Roberts, C. D.; Kazmierski, W.; Grimes, R. Preparation of biphenyls and biheteroaryls end-capped with amino acid or peptide derivatives as antivirals for treating Flaviviridae family virus infection. WO 2010/062821, 2009.
(20) Guedj, J.; Dahari, H.; Rong, L.; Sansone, N. D.; Nettles, R. E.; Cotler, S. J.; Layden, T J.; Uprichard, S. L.; Perelson, A. S. Modeling shows that the NS5A inhibitor daclatasvir has two modes of action and yields a shorter estimate of the hepatitis C virus half-life. *Proc. Natl. Acad. Sci. U.S.A.* **2013**, *110*, 3991−3996.
(21) Lemm, J. A.; O'Boyle, D.; Liu, M.; Nower, P.; Colono, R.; Deshpande, M.; Snyder, L.; Martin, S.; St. Laurent, D.; Serrano-Wu, M.; Romine, J.; Meanwell, N.; Gao, M. Identification of hepatitis C virus NS5A inhibitors. *J. Virol.* **2010**, *84*, 482−491.
(22) Targett-Adams, P.; Graham, E. J. S.; Middleton, J.; Palmer, A.; Shaw, S.; Lavender, H.; Brain, P.; Tran, T. D.; Jones, L.; Wakenhut, F.; Stammen, B.; Pryde, D.; Pickford, C.; Westby, M. Small molecules targeting hepatitis C virus-encoded NS5A cause subcellular redistribution of their target: insights into compound modes of action. *J. Virol.* **2011**, *85*, 6353−6358.
(23) O'Boyle, D. R.; Sun, J. H.; Nower, P. T.; Lemm, J. A.; Fridell, R. A.; Wang, C.; Romine, J. L.; Belema, M.; Nguyen, V. N.; Laurent, D. R.; Serrano-Wu, M.; Synder, L. B.; Meanwell, N.; Langley, D.; Gao, M. Characterizations of HCV NS5A replication complex inhibitors. *Virology* **2013**, *444*, 343−354.
(24) Tellinghuisen, T. L.; Marcotrigiano, J.; Rice, C. M. Structure of the zinc-finding comain of an essential replicase component of hepatisis C virus reveals a novel fold. *Nature* **2005**, *435*, 374−379.
(25) Love, R. A.; Brodsky, O.; Hickey, M. J.; Wells, P. A.; Cronin, C. N. Crystal structure of a novel dimeric form of NS5A domain I protein from hepatitis C virus. *J. Virol.* **2009**, *83*, 4395−4403.
(26) Penin, F.; Brass, V.; Appel, N.; Ramboarina, S.; Montserret, R.; Ficheux, D.; Blum, H. E.; Bartenschlager, R.; Moradpour, D. Structure and function of the membrane anchor domain of hepatitis C virus nonstructural protein 5A. *J. Biol. Chem.* **2004**, *279*, 40835−40843.
(27) Fridell, R. A.; Qiu, D.; Valera, L.; Wang, C.; Rose, R. E.; Gao, M. Distinct functions of NS5A in hepatitis C virus RNA replication uncovered by studies with the NS5A Inhibitor BMS-790052. *J. Virol.* **2011**, *85*, 7312−7320.
(28) Chen, P.; Couch, R.; Duan, M.; Grimes, R. M.; Kazmierski, W. M.; Norton, B. A.; Tallant, M. Preparation of biphenyls end capped with amino acids or peptide derivatives for treating HCV infection. WO 2011/028596, 2010.
(29) Baskaran, S.; Botyanszki, J.; Cooper, J. P.; Duan, M.; Kazmierski, W. M.; Mcfadyen, R. B.; Redman, A. Preparation of phenylene, pyridinylene, furanylene and thiofuranylene linked benzimidazoles and derivatives end capped with peptide derivatives for treating HCV infection. WO 2011/050146, 2010.
(30) Baskaran, S.; Dickerson, S. H.; Duan, M.; Kazmierski, W. M.; McFadyen, R. B. Preparation of naphthalenylene, quinolinylene and isoquinolinylene linked benzimidazole-imidazoles and analogs end capped with peptide derivatives for treating HCV infection. WO 2011/091446, 2011.
(31) Wang, C.; Huang, H.; Valera, L.; Sun, J.-H.; O'Boyle, D. R., II; Nower, P. T; Jia, L.; Qiu, D.; Huang, X.; Altaf, A.; Gao, M.; Fridella, R. A. Hepatitis C virus RNA elimination and development of resistance in replicon cells treated with BMS-790052. *Antimicrob. Agents Chemother.* **2012**, *56*, 1350−1358.
(32) Siebum, A. H. G.; Woo, W. S.; Raap, J.; Lugtenburg, J. Access to any site-directed isotopomer of methionine, selenomethionine, cysteine, and selenocysteine—use of simple, efficient modular synthetic reaction schemes for isotope incorporation. *Eur. J. Org. Chem.* **2004**, *13*, 2905−2913.
(33) Henriksen, B. S.; Anderson, J. L.; Hrycyna, C. A.; Gibbs, R. A. Synthesis of desthio prenylcysteine analogs: sulfur is important for biological activity. *Bioorg. Med. Chem. Lett.* **2005**, *15*, 5080−5083.
(34) Sóti, F.; Kajtár-Peredy, M.; Keresztury, G.; Incze, M.; Kardos-Balogh, Z.; Szántay, C. Synthesis of vinca alkaloids and related compounds. LV. Synthesis of (±)-desmethoxy cuanzine. *Tetrahedron* **1991**, *47*, 271−296.
(35) Walker, J.; Crosby, R.; Wang, A.; Woldu, E.; Vamathevan, J.; You, S.; Voitenleitner, C.; Remlinger, K.; Duan, M.; Kazmierski, W.; Hamatake, R. Preclinical characterization of GSK2336805, a novel inhibitor of hepatitis C virus replication that selects for resistance in NS5A. *Antimicrob. Agents Chemother.* **2014**, *58*, 38−47.
(36) Spreen, W.; Wilfret, D.; Bechtel, J.; Adkison, K. K.; Lou, Y.; Jones, L. Willsie, S. K.; Glass, S. J.; Roberts, C. D. GSK2336805 HCV NS5A inhibitor demonstrates potent antiviral activity in chronic genotype 1 infections: results from a first time in human (FTIH) single and repeat dose study. Presented at the 62nd Annual Meeting of the American Association for the Study of Liver Diseases, San Francisco, CA, U.S., Nov 6−9, 2011; *Hepatology*, **2011**, *54*, 400A.